DANISH METEOROLOGICAL INSTITUTE

——— SCIENTIFIC REPORT ———

02-09

Enhanced description of the wind climate in Denmark for determination of wind resources

Final report for 1363/00-0020
Supported by the Danish Energy Authority

Kai Sattler, Jun She,
Bent Hansen Sass, Leif Laursen

Lars Landberg, Morten Nielsen

Henning S. Christensen

COPENHAGEN 2002

ISSN Nr. 0905-3263 (printed)
ISSN Nr. 1399-1949 (online)
ISBN-Nr. 87-7478- 461-7

Enhanced description of the wind climate in Denmark for determination of wind resources

Forbedret beskrivelse af vindklimaet i Danmark med henblik på bestemmelse af vindressourcerne

Final Report for 1363/00-0020
Supported by the Danish Energy Agency

Kai Sattler, Jun She,
Bent H. Sass and Leif Laursen

Danish Meteorological Institute

Morten Nielsen and Lars Landberg

Risø National Laboratory

Henning S. Christensen

Eltra

Abstract

The wind resources in Denmark have been investigated with emphasis on the development of improved methods for making accurate wind predictions. Major efforts have been spent on developing a coupling of a complete atmospheric forecast model (DMI-HIRLAM) with an ocean wave model (WAM) based on a solution of the spectral wave energy equation. The underlying strategy is to better describe the variable frictional effects depending on the wave state of the ocean surface. The modified surface fluxes of momentum, heat and moisture are likely to have impact on the near surface wind profiles and possibly on the forecasted synoptic scale pressure systems. Many experiments have been carried out to assess the effect of partial or full coupling between the atmospheric model and the wave model. When full interactive coupling operates the wave model supplies a Charnock coefficient depending on the ocean wave stress. In turn the atmospheric model provides either a 10 metre wind, a friction velocity or the surface stress to drive the ocean wave model.

The results obtained in the project show that the effect of the coupling of DMI-HIRLAM and WAM is positive, although quite modest in its present form. It is found that the improvement increases as the horizontal model resolution is increased, and wind biases are reduced in the fully coupled runs. Also the results indicate that synoptic scale forecast improvements are best achieved if the coupling is implemented for a large model domain. The impact of increased vertical resolution appears to be more marginal. The predicted wind profiles are sensitive to other parts of the atmospheric model system such as the turbulence parameterization used in the model. It is verified that a modified turbulence scheme in its current stage improves the representation of the vertical wind profile in the atmospheric boundary layer. However, a drawback is seen on the synoptic scale surface pressure. The results of a coupling experiment over a 5 month long test period indicate that the effect of wave coupling on wind (and wind power) prediction may be larger over the ocean than over land. This supports the conclusion that a coupled atmospheric-wave model is beneficial and probably required for accurate prediction of wind over the ocean.

Another task of the project has been to investigate whether wind turbine power production may predict surface winds. A new methodology based on conditional probabilities has been developed for this purpose. A conditional wind speed distribution is assessed by Bayes rule using the probability distribution of expected power production on wind speed. The impact of the new method has been tested on data from the Abild wind farm. This test has confirmed that it is possible to improve the a priori atmospheric forecast from DMI-HIRLAM by utilizing the knowledge of the current wind power production.

Sammenfatning

Vindressourcerne i Danmark er blevet undersøgt, med hovedvægten lagt på udviklingen af forbedrede metoder til nøjagtige vindprognoser. Et større udviklingsarbejde har været nødvendigt for at muliggøre etablering af et koblet prognosesystem bestående af et atmosfæreprognosesystem (DMI-HIRLAM) og en bølgemodel (WAM) for oceanet. Sidstnævnte model er baseret på en løsning af den spektrale bølgeenergiligning for oceanet. Den underliggende strategi er at forbedre beskrivelsen af en variabel friktion ved havoverfladen. Formuleringen er afhængig af bølgetilstanden på havoverfladen. De ændrede overfladeflukse af impuls, varme og fugtighed kan forventes at have indflydelse på de vertikale vindprofiler og i et vist omfang på udviklingen af de synoptiske tryksystemer. Mange eksperimenter er blevet udført for at fastslå effekten af en delvis eller fuld kobling mellem atmosfæremodellen og bølgemodellen. Ved fuld interaktiv kobling overføres en Charnock parameter fra bølgemodellen til atmosfæremodellen. Denne parameter er afhængig af bølgemodellens bølgestress. Tilsvarende overføres fra atmosfæremodellen enten vinden i 10 meter, friktionshastigheden eller overfladestresset til bølgemodellen.

Resultaterne fra projektet viser, at effekten af at koble atmosfæremodel og bølgemodel er positiv. Indvirkningen har dog indtil videre været beskeden. Kvalitetsforbedringen på vindprognoserne viser sig at være mere markant når modellens horisontale opløsning forbedres, og modellens systematiske fejl reduceres. Endvidere viser eksperimenterne, at de bedste resultater fås når koblingen foretages på et stort modelområde. Indvirkningen af at øge den vertikale opløsning ser ud til at være mere marginal. De forudsagte vindprofiler er følsomme overfor andre dele af det atmosfæriske prognosesystem, eksempelvis over for den anvendte turbulensbeskrivelse. En ændret udgave af turbulensparametriseringen har vist sig at medføre en forbedret repræsentation af det vertikale vindprofil i atmosfærens grænselag. Den ændrede turbulensbeskrivelse har dog foreløbigt en negativ effekt på forudsigelsen af overfladetryk i modellen. Resultater fra et koblingseksperiment over en 5-måneders testperiode antyder, at effekten af bølgekobling på forudsigelse af vind (og vindkraft) vil være større over hav end over land. Det understøtter den hypotese, at en koblet model er gavnlig og sandsynligvis nødvendig ved en nøjagtig beskrivelse af vindforholdene over hav.

En anden del af projektet har bestået i at undersøge hvorvidt energiproduktionen fra vindmølleparker kan bruges ved forudsigelsen af vinde nær jord/hav-overfladen. En ny metode baseret på anvendelse af betingede sandsynligheder er blevet udviklet til dette formål. En betinget vindhastighedsfordeling fastlægges ved Baye's regel, idet sandsynlighedsfunktionen for den forventede energiproduktion som funktion af vinden anvendes. Indvirkningen af den nye metode anvendt på Abild vindmøllepark undersøges. En sådan test har bekræftet, at det er muligt at forbedre en a priori vindprognose fra atmosfæremodellen ved at anvende kendskabet til den løbende energiproduktion fra vindmøllerne.

Contents

1. Introduction

The overall goal of the project is to enhance the knowledge of the wind conditions in the lowest few hundred metres of the atmosphere over Danish land and sea territory. This knowledge is fundamental with respect to an optimal estimate of energy production from wind turbine farms. Knowledge about the wind conditions may be looked at from a climatological point of view or from a 'real time prediction' view.

A detailed climatological knowledge facilitates optimal decisions on the geographical location of new wind turbine parks. A substantial knowledge of the wind climate across Denmark has been established in recent years. The most recent and very detailed study of the wind resorce in Denmark has been carried out by Risø and EMD , see www.emd.dk/ for further details.

The first systematic study of the wind resource was done in 1981, when the wind was derived from the synoptic pressure field (Lundtang et al., 1981). This study was followed by the European Wind Atlas (Troen and Petersen, 1989) in which the Wind Atlas Methodology was developed. The methodolgy is implemented in the WASP program (www.wasp.dk). WASP is by many considered the industry standard for wind resource estimation, see Mortensen et al. (2002) for further details.

In order to make energy production from wind turbine parks useful in the management of energy supply to customers on a large regional scale, it turns out that the wind conditions need to be forecasted with some skill in real time for the region under consideration. Otherwise it is not known how much of the traditional energy production can be replaced by wind energy on a time scale of a few hours to a few days. As a consequence, accurate wind forecasts by operational meteorological models are needed.

At the Danish Meteorological Institute (DMI) an atmospheric model prediction system DMI-HIRLAM (Sass et al., 2002) has been operational since 1991 and is further developed in an international collaboration (Undén et al., 2002). In order to be successful in real time, this system has an advanced system for assimilating meteorological data and a forecast model which treats both the dynamical and the physical processes in the atmosphere in detail.

The valuable information of real time wind prediction from the operational atmospheric model at DMI has been demonstrated in the context of wind energy production in a previous study carried out by Risø, DMI and the electricity companies ELKRAFT and NESA (see Landberg et al. 1997).

Besides real time predictions the DMI-HIRLAM model system has potential for re-analysing the wind climate in Denmark in combination with local wind adaptation modules such as WA^{s}P. Such re-analysis of wind climate has been planned to be part of the present project.

However, the improved model system developed during the project, and the requirements for large experiments, e.g. involving model integrations on a big model domain with full coupling to an ocean wave model, has made this type of study excessively demanding with the available computer resources during the project period. As a consequence, the studies carried out have put most emphasis on the problems related to real time forecasting of wind and the associated energy production. In particular, studies have been carried out to evaluate the results obtained with a more realistic description of the momentum exchange between the sea surface and the overlying atmosphere (see section 2). More specifically, a wave model for the ocean has been

coupled interactively with the DMI-HIRLAM model. The reasoning behind this strategy is that recent results elsewhere, e.g. at the European Centre for Medium Range Weather Forecasts (ECMWF) indicate an increased skill for wind (and wave) forecats by an interactive coupling of the two systems (e.g., Janssen et al. 2001).

It is important to realize that a modest improvement in the wind prediction may lead to a significant improvement of the energy production from wind turbines. This is because of a steep slope of the 'power curves' (defining the basic transformation between wind and energy production) in the range of typically 7 - 12 m/s. This range obviously represents a modest wind interval, and therefore rather small changes in wind speed can have significant effects on the energy production. A goal of this project is to achieve an improved skill of about 4 percent on predicting the energy production in the western part of Denmark.

Another important topic is the specific estimates of wind and energy production for wind farms over land. Two specific studies have been carried out in this context. The first one concerns a wind farm in southern Jutland. A new method has been developed for improving the wind estimates by combining DMI-HIRLAM forecasts with WA^{s}P and actual energy production for the site.

Another study has been carried out with DMI-HIRLAM where power production estimates have been made for 4 wind turbine parks on the coasts of Jutland. Results have been studied with and without interactive coupling between the wave model (WAM) and DMI-HIRLAM to investigate the impact of the coupling over sea on wind prediction over land.

The developments related to coupling between the wave model and DMI-HIRLAM are described in section 2 which also describes results of various tests using different coupling strategies.

The developments for wind and energy production over land are described in section 3. In all cases where information from wind turbines has been involved, the independent system operator and transmission company ELTRA has kindly supplied the relevant data.

Finally section 4 contains conclusions and outlook for the future.

2. Wind forecasting over sea

Information on the wind conditions over sea is not only relevant to the ship traffic. Many other important activities rely on wind information. The energy production from wind turbines is a key issue in the present project, and in recent years it has been feasible to install large wind mill parks at sea. Several such parks have already been establised in Danish domestic sea areas, e.g. in the Wadden Sea (Horn's Rev) and in Kattegat south of Læsø.

It is advantageous to establish wind turbines at sea, because winds are often stronger over sea as compared to over land. This is connected to a smaller momentum transfer over a sea surface, but the wind conditions in coastal regions are often complex due to the presence of land nearby with changing surface characteristics. The Danish domestic waters is a good example where a complex coastline and many islands influence the wind conditions.

The prediction of energy production from a wind turbine typically requires information on wind

speed and direction up to about 100 metres above the sea surface. The detailed wind information over sea can be provided by meteorological models. In this project DMI-HIRLAM is used. The forecasts of wind require not only that proper analyses of the atmospheric state can be made, but also that the physics and dynamics of the model are realistic.

The momentum, heat and moisture transfer at the sea surface and the fluxes through the planetary boundary layer are important features of the model which influence the wind profiles and the model forecasts.

The present study investigates the possible improvements of model winds over sea, as a result of interaction between the atmospheric model and an ocean wave model. The reasoning is that the atmospheric state and the state of the ocean surface are not independent, but interact. In recent years there has been a considerable interest to investigate how much this interaction between wind and ocean waves influences the wind forecasting over sea.

Experimental evidence has shown (Donelan, 1982; Smith et al., 1992) that, especially for young wind sea, the air flow depends on the sea state. Examples comprise the air flow near fronts and in coastal regions for offshore wind directions. The drag coefficient may vary by a factor of two between young and old wind sea cases. This suggests that it is important to regard the interaction process between wind and waves as a two-way process: The wind generates the waves which feed back on the atmospheric flow. Parallel to this development a theory of two-way interaction between wind and waves was developed, giving the sea state dependence of momentum, heat and moisture transfer (Chalikov and Makin, 1991).

It turns out that an elaborate wave model is needed in the context of atmosphere-ocean interaction. As a consequence, an international group of scientists, the socalled Wave Modelling Group (WAM) was established. The group developed a realistic wave model in the 1990s (Komen et al., 1994).

The most advanced operational atmospheric models, e.g. the ECMWF (= European Centre for Medium range Weather Forecasts) global model has demonstrated some skill when implementing a coupling of WAM with the operational atmospheric forecast model. The first coupled version (1998) showed little impact of coupling. However, improved versions of the wave model combined with increased resolution in the atmospheric model has lead to significant model improvements (Janssen et al., 2001). These findings provide important arguments for testing a coupled wave-atmosphere model where DMI-HIRLAM is run at a relatively high model resolution.

The parts of DMI-HIRLAM relevant to define the coupling and the fluxes of momentum, heat and moisture are described in section 2.1. A version of the wave model mentioned above which is used operationally at DMI is described in section 2.2. The coupling methods are defined in section 2.3. From a practical point of view a good implementation of the coupling of WAM and DMI-HIRLAM has been technically demanding since the interface needs to be efficient and realistic, allowing for interaction between the two models every time step. Experiments related to coupling and wind forecasts over sea, including results, are described in section 2.4. A coupling experiment concerned mainly with wind and energy production over land is described in section 3.4.

2.1. DMI-HIRLAM

The atmospheric model DMI-HIRLAM is a numerical weather prediction model used operationally at the Danish Meteorological Institute (DMI). HIRLAM stands for 'HIgh Resolution Limited Area Model'. The model originates from the international HIRLAM collaboration (Machenhauer, 1988; Källén, 1996; Undén et al., 2002). Some model components in the DMI-HIRLAM have been specifically developed for DMI opertaional activity and research prrojects. A description of the model system is available (Sass et al., 2002).

2.1.1. Model description

The model is based on the the hydrodynamical equations of the atmosphere, the equation of continuity for atmospheric constituents including moisture variables, the equation of state for atmosheric air and the first law of thermodynamics. In addition, for the present hydrostatic model, the hydrostatic relation between increments of geopotential and pressure is utilized. The prognostic variables comprise surface pressure, p_s, the horizontal wind components (u,v) temperature (T), specific humidity (q), specific cloud condensate (q_c) and subgrid scale turbulent kinetic energy (E).

The numerical model is based on finite differences on a staggered grid. The dynamics are of Eulerian type consisting of an explicit part and a semi-implicit part. Optionally a semi-Lagrangian advection scheme may be used. In the model, a horisontal diffusion is applied which prevents spurious accumulation of energy on the smallest scales. The lateral boundary condition represents a dynamical forcing which is treated by a specific boundary relaxation scheme.

In addition, the relevant physical processes (radiation, surface processes, turbulence, condensation and precipitation) are described by detailed parameterizations. Optionally the model can be run with a longer time steps for the physical processes than used for the model dynamics. In this case the model physics is affected by the dynamics through time averaging during the dynamical sub-steps.

As regards wind forecasting over sea (and land) the key processes are the surface fluxes of momentum, heat and moisture. In addition, the model's turbulence scheme is essential because it is reponsible for the vertical distribution of momentum in the atmosphere and hence the wind profiles. The heat and moisture transports by turbulence are also vital for the energetics of the weather prediction model and has an indirect effect on the momentum flux at the sea surface.

Turbulent surface fluxes in numerical weather prediction models are traditionally computed from drag formulae relating the surface fluxes to the mean states of the surface and of the atmosphere at the observation height (in a numerical model, typically the lowest model level). The drag coefficient C_γ for a scalar variable γ is defined by the equation

$$\overline{w'\gamma'} = C_\gamma \Delta\gamma |\vec{V}_N| \tag{1}$$

in which $\overline{w'\gamma'}$ is the vertical turbulent kinematic flux of γ and $\Delta\gamma = \gamma_s - \gamma_N$. Finally, $\vec{V}_N$ equals the horizontal wind speed at the lowest model level. N is the number of vertical model

levels.

The scalar variables and the wind vector $\vec{V}_N$ on the right hand side of (1) are time averages like the flux term on the left hand side, but for convenience the averaging symbol has been omitted on the right hand side. The sign convention in (1) is such that upward fluxes are positive.

Over the ocean $\vec{V}_N$ should, strictly speaking, be measured in a frame moving with the ocean surface current and T_s should be the surface skin temperature.

The surface wind speed $\vec{V}_s$ may be assumed to be zero and it is assumed that the saturation value $q_{sat}(T_s)$ with respect to the surface temperature applies.

In the current formulation

$$C_\gamma = C_{MN}\left(1 + \ln\frac{z_{0M}}{z_{0H}}\Big/\ln\frac{z}{z_{0M}}\right)^{-1}\Psi_\gamma\left(Ri, \frac{z}{z_{0H}}, \frac{z}{z_{0M}}\right) \tag{2}$$

This formulation is used for different surface types and forecast scalar parameters. ($\gamma = M$ for momentum, correspondingly H and Q stand for heat and moisture transfer, respectively). The two factors in front of the function Ψ_γ form a neutral drag coefficient C_{γ_N}. For identical roughness lengths z_{0M} and $z_{0\gamma}$ the second factor in the brackets becomes unity and $C_{\gamma_N} = C_{MN}$.

$$C_{MN} = \Big(\frac{k}{\ln(\frac{z}{z_{0M}})}\Big)^2$$

$k \sim 0.4$ is the von Kármán constant.

The functions used for Ψ_γ follow the work of (Louis, 1979) and (Louis et al., 1982).

The following form applies to the unstable atmospheric boundary layer:

$$\Psi_\gamma = 1 + \frac{a_{\gamma_U} Ri}{1 + b_{\gamma_U} C_{\gamma_N} (Ri\frac{z}{z_{0M}})^{\frac{1}{2}}} \tag{3}$$

In (3) above Ri is the surface bulk Richardson number. $a_{mU} = 10$, $b_{mU} = 75$, $a_{HU} = a_{QU} = 15$ and $b_{HU} = b_{QU} = 75$.

The special situation when the mean horizontal wind speed goes to zero in an unstable boundary layer is described in Sass et al. (2002)

For the stable boundary layer the corresponding formulas are

$$\Psi_M = \frac{1}{1 + \frac{a_{MS} Ri}{\sqrt{1 + b_{MS}\, Ri}}} \tag{4}$$

In (4) above $a_{MS} = 10$, $b_{MS} = 1$.

For heat and moisture the following function is used

$$\Psi_\gamma = \frac{1}{1 + a_{\gamma S} Ri\sqrt{1 + b_{\gamma S} Ri}} \tag{5}$$

$a_{HS} = a_{QS} = 10$ and $b_{HS} = b_{QS} = 1$.

To complete the parameterization for surface flux computations over sea the ratio of the roughness lengths z_{0M}/z_{0H} and z_{0M}/z_{0Q} must be related to known quantities. Measurements over sea indicate that the surface roughness lengths for momentum, sensible heat and moisture are different, (DeCosmo et al., 1996). The main reason is probably that form drag (i.e., momentum transport by pressure forces) in the presence of sea waves enhances the momentum transfer, while the heat and moisture transfers at the air-sea interface are controlled by molecular diffusion alone.

According to observations and laboratory experiments z_{0M} depends on the sea state. At low wind speeds laboratory experiments indicate that the sea surface becomes aerodynamically smooth with z_{0M}=$0.11\,\nu/u_*$. At sufficiently high wind speeds the sea surface becomes aerodynamically rough. In the latter conditions the Charnock formula $z_{0M} = \beta u_*^2/g$, (Charnock, 1955) is used. In numerical models of the atmosphere values of β in the interval 0.014 to 0.0185 have been recommended (Garrat, 1992). The present study allows for an interactive computation of β when coupling to WAM is switched on.

We introduce a transition in z_{0M} from a smooth to a rough sea surface depending on wind speed $|\vec{V}_N|$. The interpolation formula for z_{0M} is specified as

$$z_{0M} = (1 - \xi(\mathrm{u}))\, 0.11\,\nu/u_* + \xi(\mathrm{u})\beta\frac{u_*^2}{g}\,, \tag{6}$$

with

$$\xi(\mathrm{u}) = \left[\max\left(\min\left(\frac{u - u_s}{u_r - u_s}, 1\right), 0\right)\right]^{1/2}\,. \tag{7}$$

In (6) and (7) $u = |\vec{V}_N|$, $u_s = 3.0$ m/s and $u_r = 5.0$ m/s. According to (6) and (7) the sea surface is considered to be smooth for $u \leq 3$ m/s and rough for $u \geq 5$ m/s. The transition interval is somewhat smaller than the interval from 2.5 to 5.5 m/s usually found in the literature e.g., (Garrat, 1992).

When there is no interactive coupling to WAM the following simplified formulation is used. Over open sea (here defined as fraction of sea in a model grid equal to 1) β has been set to 0.014, otherwise $\beta = 0.032$. A higher value of β (larger momentum flux) in shallow coastal waters is supported by measurements (Oost, 1998; Hansen and Larsen, 1997; Maat et al., 1991), although the governing parameter for z_{0M} seems to be the wave age.

We assume that z_{0H} and z_{0Q} can be related to z_{0M}. Observational evidence of a relation between z_{0M} and z_{0Q} has been presented for example by DeCosmo *et al.*, 1996. Dependence of z_{0H} and z_{0Q} on z_{0M} are also key features in 'surface flux over sea' models by e.g. (Clayson et al., 1996; Liu et al., 1979; Brutsaert, 1975). In our parameterization z_{0H} and z_{0Q} are related to z_{0M} by formulae suggested in Garrat, 1992. In terms of the roughness Reynolds number, Re_*, the relations take the form

$$\ln\frac{z_{0M}}{z_{0H}} = \alpha_H Re_*^{1/4} - 2\,, \tag{8}$$

$$\ln\frac{z_{0M}}{z_{0Q}} = \ln\frac{z_{0M}}{z_{0H}} - \alpha_Q Re_*^{1/4}\,, \tag{9}$$

in which Re_* is defined as

$$Re_* = \frac{z_{0M}u_*}{\nu}\,, \tag{10}$$

i.e., by the sea surface momentum roughness length (z_{0M}), the surface friction velocity (u_*) and the molecular kinematic viscosity coefficient for air ($\nu \simeq 1.5 \cdot 10^{-5}\,\mathrm{m^2/s}$). Over a rough sea α_H=2.48 and α_Q=0.2. With the transition from a smooth to a rough sea surface given by (7), and over a smooth surface with the requirement $z_{0\gamma} \cdot u_*/\nu = S_\gamma$ for $\gamma = H, Q$ and $S_H \approx 0.2$ and $S_Q \approx 0.3$ (Garrat, 1992), the coefficients α_H and α_Q in (8) and (9) become

$$\alpha_H = 0.05\xi(\mathrm{u}) + 2.43\,, \tag{11}$$

$$\alpha_Q = -0.50\xi(\mathrm{u}) + 0.70\,. \tag{12}$$

The turbulence scheme (Cuxart et al., 2000; Sass et al., 2002) is formulated in the framework of 'turbulent kinetic energy' (E) as a prognostic variable. This means that a specific prognostic equation is solved for E. The terms include the production of turbulent kinetic energy due to wind shear, buoyancy, vertical transport of E arising from turbulence and dissipation of E. Also the advection of E by the large scale flow is considered. Two terms have been neglected in the production equation for E. The first term involves vertical velocity variance in the wind shear production. The second term describes the effect of pressure correlations.

The parameterization of the turbulent transports relates the second order moments to mean variables by assuming relations of the form

$$-\overline{\zeta' w'} = K_\zeta \left(\frac{\partial \overline{\zeta}}{\partial z}\right); \quad \zeta = u, v, \theta, q, q_c, E. \tag{13}$$

In (13) K_ζ is an eddy exchange coefficient analogous to the molecular viscosity and diffusivity coefficients. θ is the potential temperature. The eddy exchange coefficients depend on $\overline{E}$:

$$K_\zeta = c_\zeta K_u \phi_3\,(Rs)\,, \tag{14}$$

where c_ζ is a non-dimensional constant and $K_u = l\sqrt{\overline{E}}$ is the eddy exchange coefficient for momentum.

l is a diagnostic mixing length. It is computed from

$$l = \sqrt{l_u \cdot l_d}, \tag{15}$$

where l_u and l_d are the distances an air parcel must be displaced upward or downward, respectively, before its $\overline{E}$ has been consumed by buoyancy. This formulation allows for diagnosing very large mixing lengths in neutral or unstable stratification. Currently the following constraint is imposed near neutral atmospheric stratification.

$$l = \min\{l, l_{max1} + (l_{max2} - l_{max1})\exp(-\frac{z^{'} - H_{pbl}}{H_{pbl}})\} \tag{16}$$

In (16) H_{pbl} is the planetary boundary layer height used in the model (Sass et al., 2002). $z^{'} = \max\{z, H_{pbl}\}$. Currently $l_{max1} = 100$ m, $l_{max2} = 500$ m.

ϕ_3 is a function of the dry Redelsperger number Rs

$$Rs = \frac{g}{\overline{\theta_v}} \frac{l^2}{\overline{E}} \left(1 + 0.61\,\overline{q} \frac{\partial \overline{\theta}}{\partial z} + 0.61\,\overline{\theta} \frac{\partial \overline{q}}{\partial z} \right). \tag{17}$$

In (17) θ_v is the virtual potential temperature. ϕ_3 takes the form (Cuxart et al., 1995)

$$\phi_3 = (1 + 0.139 \cdot Rs)^{-1}, \tag{18}$$

where Rs is controlled by the condition $Rs = \max\{-3.924, \min\{Rs, 71935.252\}\}$.

A diagnostic lower boundary condition is specified for $\overline{E}$ at the bottom level (index N). It is specified as

$$\overline{E}_N = 3.75 u_*^2 + \delta_u \left[u_*^2 \left(-\frac{z_N}{L} \right)^{2/3} + 0.2 w_*^2 \right], \tag{19}$$

with $\delta_u = 1$ or 0 if the surface layer is unstably or stably stratified, respectively. In the equation above L is the Monin-Obukov length scale (Businger et al., 1971). w_* is the convective velocity scale (Deardorff, 1972) and u_* is the friction velocity.

2.1.2. Uncoupled weather model results

An indication of the typical forecast accuracy obtained for 10m wind speed with the different operational DMI-HIRLAM versions are presented in Fig. 1. The upper panels apply to the first quarter of 2002 while the lower panels display the corresponding reults for the second quarter of 2002. Statistics for bias and standard deviation are computed as separate averages for 13 Danish meteorological coastal stations (left panels) and 13 synoptic land stations (right panels) The horizontal resolutions associated with models G45, D15 and D05 are, respectively, 0.45 °, 0.15 ° and 0.05 °. These statistics apply to DMI-HIRLAM when not coupled to a wave model.

It is seen that statistics generally vary between different 3 month periods. The systematic errors are generally smaller in the high resolution runs (”D15” and ”D05”) as compared to ”G45”. The standard deviations are quite similar for coastal stations, but tend to be smaller over land as the resolution of the model increases.

2.2. Wave model

Many operational wave models are based on *WAM Cycle4*, a 3rd generation research wave model developed by the WAM Group since 1991 (Komen et al., 1994; Günther et al., 1992). The latter of these publicalions provides a technical model description. WAM is used in numerous applications thoughout the world, both in operational wave forecasting services and for scientific investigations. The DMI Weather Service Department has used this model to produce high resolution wave forecasts for Danish waters since 1999 - a service later extended to include the full NW European shelf region and the Mediterranean.

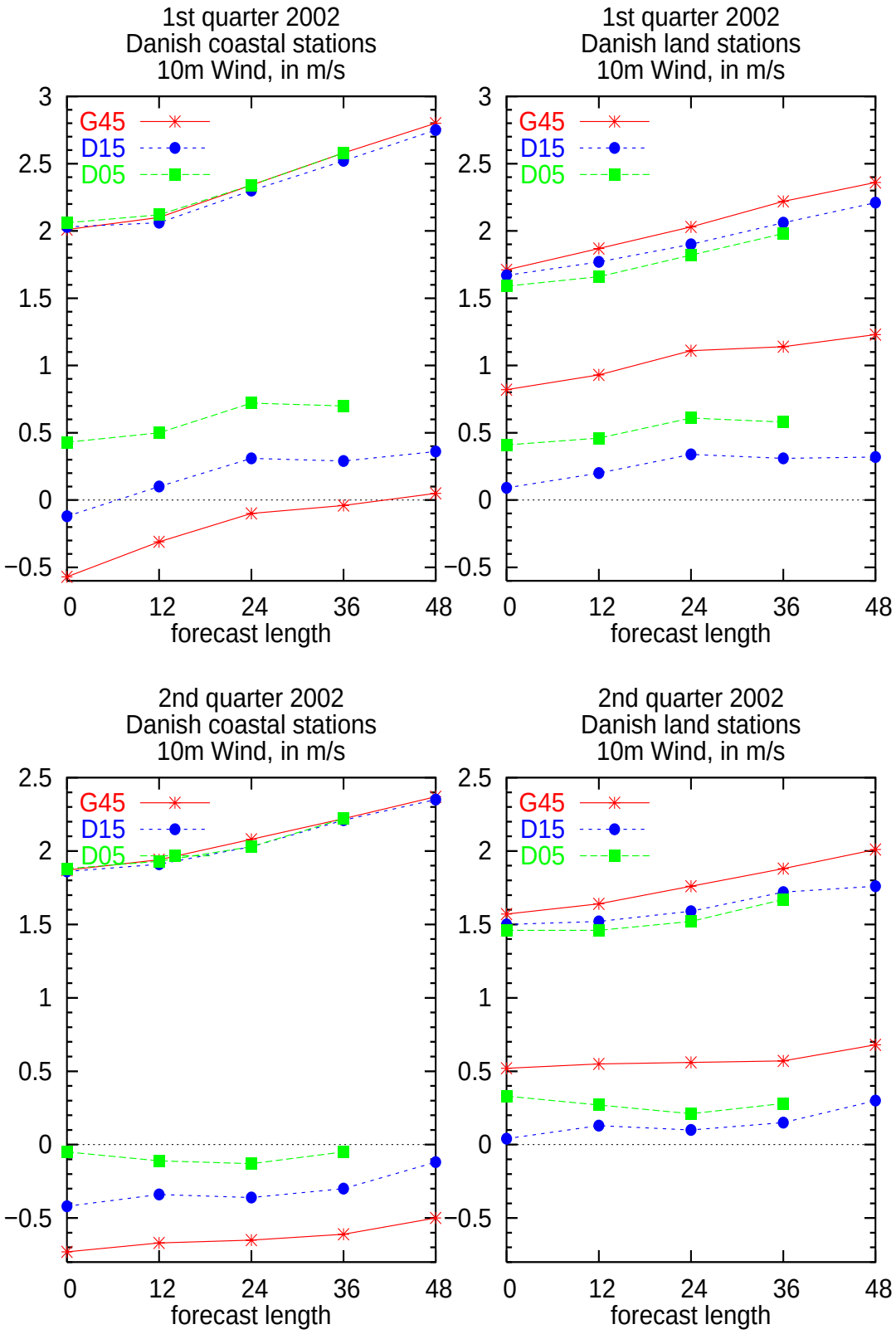

Figure 1: Operational results (bias and rms) for 10m wind in the first and second quarter of 2002. Left columns shows average results for 13 coastal stations and right column shows results for 13 land stations.

2.2.1. Model description

WAM Cycle4 solves the spectral wave energy equation

$$\frac{\partial F}{\partial t} + \vec{c_g} \cdot \vec{\nabla} F \quad = \quad S \tag{20}$$

where $F(f, \theta; \vec{x}, t)$ is the spectral wave energy density, depending on wave frequency, wave direction, position and time; $c_g(f, \theta)$ is the wave group speed; The source term S includes wind energy input, non-linear wave-wave interaction, wave energy dissipation through wave breaking (white capping), wave-current interaction and interaction with the sea bed through friction and wave refraction.

Each of the source term contributions has been carefully parameterized by the WAM group. In contrast to 1st and 2nd generation models, the 3rd generation model WAM introduces no ad hoc assumptions on the spectral shape, and non-linear wave-wave interaction is calculated explicitly.

WAM Cycle4 is a grid point model, operating on the water points of a regular spherical grid. The polar singularity is not considered since none of the poles have open water. The model typically has $\sim$300-700 variables per wet grid point - making it comparable in size to a numerical weather prediction (NWP) model. The model steps forward in time using a simple Euler scheme with a time step of a few minutes - depending on grid spacing - required for numerical stability. The resolution is usually a compromise between model accuracy and computing resources.

Model forcing is 10m wind as obtained from a NWP model. Alternatively, surface stress τ or friction velocity u_* may be specified; WAM transforms this into a wind speed using

$$U_{10} = u_* / C_D \tag{21}$$

with

$$u_* = \sqrt{\tau / \rho_a}; z_0 = \alpha / g u_*^2; C_D = \kappa / \log \frac{10}{z_0} \tag{22}$$

where α, κ, ρ_a (air density) and g (gravity) are constants. NWP winds are interpolated linearly in time and space from any spherical grid to the WAM time-space mesh. The spectral energy input S_{in} depends both on the wind speed and the wave-induced stress. The term is given by

$$S_{in} = \gamma F \tag{23}$$

where the growth rate γ depends on the friction velocity u_* and the roughness length z_0.

As pointed out by Janssen (1999), the wave model could be viewed as a part of a weather model, providing more accurate momentum lower boundary condition through the surface roughness length z_0. The wave model may also serve as a weather model validation tool.

A global or basin model requires no further time-dependent input (depth maps being time-independent), while a regional model needs information on the the full wave spectra along open boundaries. This is provided in one of two ways; a) by nesting into a large scale model which then provides the spectra, or b) a parameterized JONSWAP wind-sea spectrum is diagnosed from 10m wind and fetch along the boundaries (K. Hasselmann et al., 1973). In the latter case, the model lacks prescribed swell energy generated outside the model domain.

A WAM Cycle4 wave prediction may be 'cold started', when the initial wave state is parameterized by the JONSWAP spectrum, depending on local wind and fetch. The model spin-up time ranges from a few hours to several days, depending on the weather situation. In operational applications a "hotstart" is used, when initial wave spectra are output from a previous model run. In more advanced applications, wave height information obtained from altimetry may be assimilated into the model to improve the initial condition.

Model output are functions of the spectral wave energy density F, integrated to produce maps of wave height, period and direction. Subsets of the spectrum are integrated to produce wind sea and swell parameters.

In operational forecast applications WAM Cycle4 is often modified and elaborated according to each user's requirements. The European Center for Medium-Range Weather Forecasts (ECMWF) has operationalised a comprehensive global version, with assimilation of real-time satellite altimetry wave height products, parallel computing, and short-fetch improvements with a two-way instant coupling with the ECMWF weather model.

2.2.2. Wave predictions

WAM Cycle4 has been running operationally at DMI since 1999. Mid-2002 the DMI-WAM set-up consists of 3 model domains: 1) a coarse grid (30') model of the North Atlantic, 2) a fine grid (10') model of the Northwest European Shelf region, the North Sea and the Baltic Sea, nested into the coarse grid model, and 3) a closed (10') basin Meditteranean model. DMI-WAM uses shallow water friction and depth refraction, but no current refraction. The wave spectrum is discretized in 25 frequencies and 12 directions, and the time step is 4 minutes. A standard WAM test in a rectangular basin of constant depth shows that doubling the directional resolution reduces the significant wave height error by a few %, this improvement may be larger in near-shore regions (Bidlot et al., 1997). DMI-WAM is run 4 times a day for a 54 hour forecast, using hourly wind forcing obtained from DMI's NWP model HIRLAM in 15 km resolution where possible, and 45 km resolution elsewhere. The depth maps are based on ETOPO5, a global 5'

topography data set generated by National Geophysical Data Center *(www.ngdc.noaa.gov/)*.

WAM Cycle4 has been well calibrated in open seas, but only few studies concern short-fetch wave conditions common in the coastal zone. This matter is still not fully resolved. Using Belt Sea field campaign wave data from 1992/94, (Hansen et al., 1998) found that WAM Cycle4 over-predicted the significant wave height by 30-40$\%$ in the Belt Sea region for strong wind conditions ($U_{10} \sim 15m/s$). This result is contradicted by other results (Hersbach and Janssen, 1999), indicating under-prediction of significant wave height under restricted fetch conditions.

A calibration and validation study has been carried out using a stand-alone North Sea-Baltic Sea model forced by analysed 10m wind fields (J.She and Nielsen, 1999). The significant wave height predictions were compared with 14 buoy wave data sets (North Sea, Sound, and Baltic Proper). Observed and hindcasted significant wave height agreed well in general, with a high correlation coefficient and no bias on average. The peak waves are underestimated by $\sim$10%. There are some problems in near-shore regions (not adequately resolved by the model) and near open boundaries (due to lack of swell).

To improve model performance in the Belt Sea, where error statistics change rapidly over a small distance, a resolution of about 2.5' or better is required to resolve small islands, reduce shadow effects and get a more accurate fetch. This was not implemented due to lack of computing resources.

The northern North Sea suffered from lack of swell, leading to significant negative bias in this region. The boundary condition was improved by nesting into a coarse grid North Atlantic model, reducing the negative bias.

In the Baltic, the underestimation of high waves may be related to error in the wind forcing or the parameterisation of source terms. This needs to be further investigated.

Since primo 2002, the operational DMI-WAM is verified on a regular basis using wave bouy data and 1-54 hour forecasts from some 30 stations (Fig. 2). The results presented below stem from a two-month pilot study using data from nov-dec 2001 (Nielsen et al., 2002). We consider only significant wave height.

The model comparison with observed data has an average correlation cofficient of 0.90 (Fig. 3) and only a weak dependency of bias and rms error on forecast range. There are, however, large regional differences in forecast quality. This is presumably related to the model resolution (spectral and spatial) being inadequate in some regions. 5 stations have a scatter index larger than 0.4 (sometimes used as an acceptance level).

The model has no bias on average and an rms error of $\sim$20% (excluding very small waves). Small waves (less than about 3m) are overpredicted, while high waves (larger than 3m) are un-

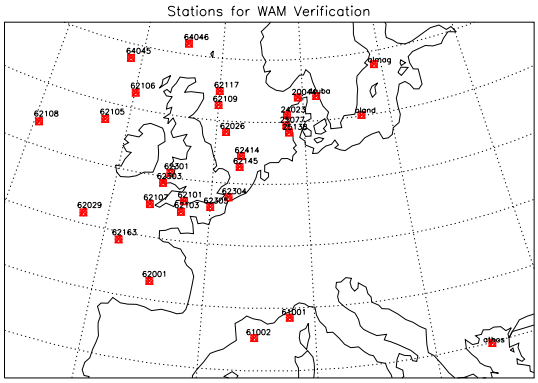

Figure 2: DMI-WAM verification stations

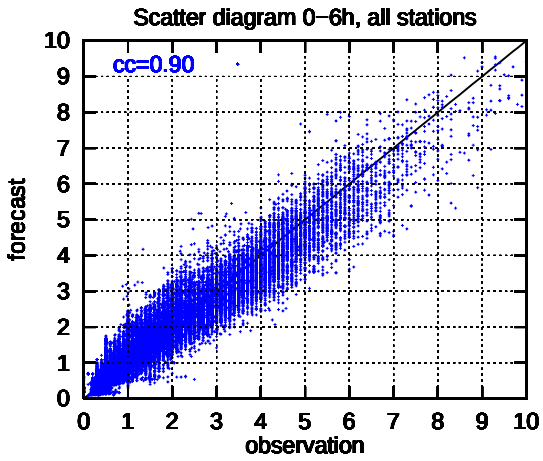

Figure 3: Observed vs. predicted significant wave height, DMI-WAM nov-dec 2001.

derestimated. The negative bias on high waves increases with wave height so that waves of 10m have a negative bias of 15% or 1.5m. This result is common for WAM applications.

The DMI-WAM is planned to be provided with an extra nesting level to improve resolution in the inner Danish waters. Directional resolution should be increased from 12 to 16 or possibly 24 directions.

2.3. Coupling Methods

2.3.1. Coupling HIRLAM and WAM

In the real atmosphere and ocean systems, the sea surface and the atmospheric boundary layer (ABL) experience a close interaction. The surface wind induces water waves on the sea surface. These waves together with existing waves in turn induce a drag on the atmospheric flow, extracting momentum from it. This in turn decreases the velocity of the air flow, which again acts

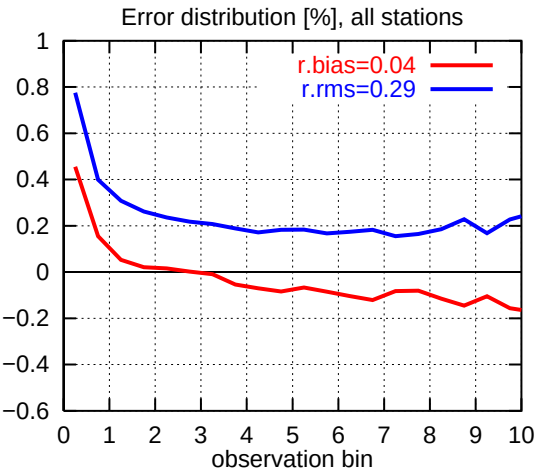

Figure 4: Bias and rms error depending on significant wave height.

on the sea waves trying to establish a quasistationary equilibrium. This state is, however, continously disturbed by sea surface wave dynamics as well as by the atmospheric dynamics and the physical processes. The aim of coupling DMI-HIRLAM and DMI-WAM is to include these interaction dynamics into the model system in an approximated way. In principle this should benefit both models.

The atmospheric model HIRLAM simulates among other parameters the wind conditions close to the surface. It is neccessary to describe the lower boundary of the model by the various properties of the surface, which have to be represented by a set of parameters. One of these parameters is the Charnock value (Charnock, 1955), which is an implicit measure of the drag over sea. It influences the low level winds in HIRLAM via the roughness length for momentum (Sass et al. 2002):

$$z_{0,sea} = \frac{\beta u_*^2}{g}, \tag{24}$$

where β is the Charnock value, u_* is the surface friction velocity and g is the gravity acceleration. In a stand-alone atmospheric model, β is a constant often set between 0.014 and 0.0185.

In the wave model WAM, the wave spectrum tendency is influenced by the low-level wind over the sea, creating the stress through a drag formulation (Günther et al., 1992):

$$\tau_a = \sqrt{C_D u(z_l)}, \tag{25}$$

where $u(z_l)$ is the low-level wind, and C_D is the drag coefficient:

$$C_D = \left(\frac{\kappa}{\ln\left(\frac{z_l}{z_{0,wam}}\right)} \right)^2. \tag{26}$$

The roughness length $z_{0,wam}$ is modeled in WAM using a stationary logarithmic wind profile:

$$z_{0,wam} = \frac{\alpha \tau_a}{g\sqrt{1 - \frac{\tau_w}{\tau_a}}}, \tag{27}$$

where τ_w is the wave induced stress and α is the Charnock value. When coupling HIRLAM and WAM, we set $z_{0,sea} = z_{0,wam}$, which relates the Charnock value representations from the two models as folllows:

$$\beta = \frac{\alpha}{\sqrt{1 - \frac{\tau_w}{\tau_a}}}, \tag{28}$$

It follows from the considerations above, that coupling between HIRLAM and WAM is realized by communicating the low-level wind $u(z_l)$ from HIRLAM to WAM, and by communicating the Charnock value β from WAM to HIRLAM. Doing this, the level z_l is usually choosen to be 10 m. As WAM also necessitates atmospheric input as a stand-alone model, it already includes a pre-processor for the low-level wind. However, it is still possible to also communicate momentum flux τ or friction velocity u_* instead of the low-level wind. WAM will then determine a representative low-level wind from these (see also eq. (21) and (22))

$$u(z_l) = \frac{u_*}{\kappa} \ln\left(\frac{z}{z_0}\right), \qquad z_0 = \frac{\alpha}{g} u_*^2 \tag{29}$$

and

$$u_* = \sqrt{\frac{\tau}{\rho_0}}, \tag{30}$$

where constant air density ρ_0 is assumed in the case of momentum flux.

2.3.2. Communication schemes HIRLAM–WAM

This section describes some of the technical aspects of the communication in the coupled model HIRLAM–WAM. In a first approach, a ”loose coupling” was applied, which consists of the following steps:

1. force WAM with winds from a stand-alone HIRLAM run and store the Charnock fields with a predefined time interval
2. rerun HIRLAM with the inclusion of the WAM Charnock fields instead of the model internal constants
3. rerun WAM with updated wind fields from the new HIRLAM run
4. etc.

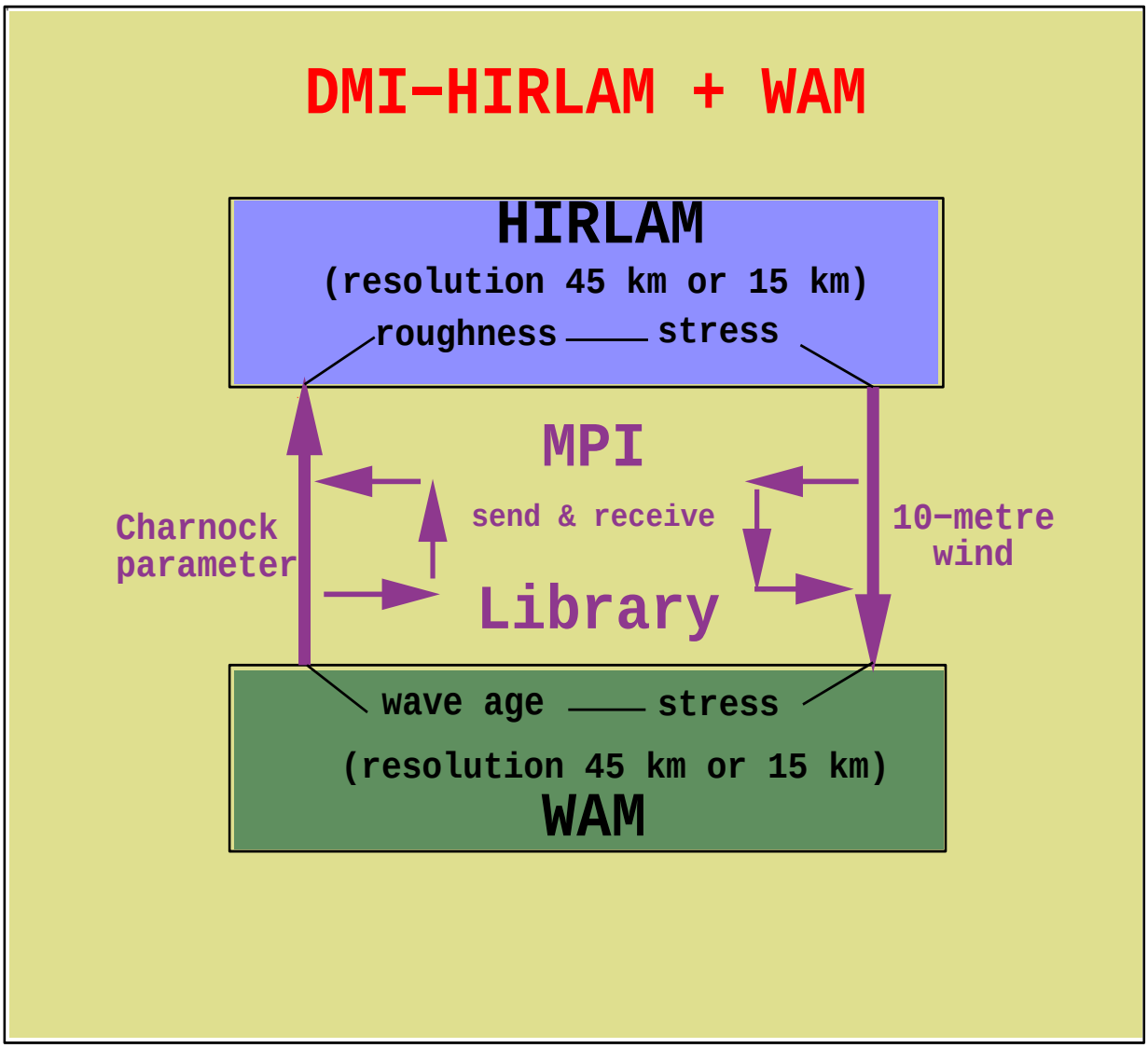

Figure 5: Schematic representation of the interactive coupling between the atmospheric model DMI-HIRLAM and the WAM.

This iterative process is fast to implement and revealed to be usefull during the first low-resolution coupling experiments. It is in the long run, however, quite tedious and not practical when increasing the horizontal resolution of the models.

In a second step, the coupling was implemented into the models via an MPI interface, making it possible for the models to communicate with a significantly higher frequency. Figure 5 depicts the principle of this scheme. The implementation is realized such that the coupling time step can be chosen arbitrarily in multiples of the largest time step in the two models.

The implementation of the coupling in both models made it necessary also to implement the possibility to change the grid of the wave model from a regular geographic grid to a rotated one, which usually is utilized in HIRLAM. This makes equality of the grids of the two models possible, which enhances the coupling quality by avoiding interpolation deviations.

2.4. Studies

2.4.1. Non-instant coupling experiments

An experiment has been made for the 4-month period November 1999 - February 2000 with a non-instant WAM-HIRLAM coupling interface. The purpose of the experiment is to test the influence of the non-instant coupling on wind and wave predictions. The following tests were run:

- *HIRLAM analysis run*
  A 14-month HIRLAM run in January 1999 - February 2000, with about 15km horizontal resolution, 6-hour forecasts and hourly wind output (uncoupled HIRLAM analysis run).

- *Uncoupled WAM run*
  A WAM run for the same 14-month period with 0.25° resolution and hourly output (including Charnock number)
  .

- *Coupled HIRLAM run*
  A 4-month (November 1999 - February 2000) HIRLAM run with sea-state dependent Charnock number from the uncoupled WAM run.

- *Coupled WAM run*
  A 4-month WAM run forced by the coupled HIRLAM run.

2.4.2. Validation of the 14-month HIRLAM and WAM runs

Outputs of the HIRLAM analysis run and the uncoupled WAM have been validated against buoy measured winds and waves in North Sea as a baseline for coupling analysis (She, 2000). Specifically the results show the following bias features of the models:

- In average the HIRLAM analysis run has a positive 10m wind speed bias of 0.64 m/s, and the related WAM run has almost no significant wave height bias.
- Seasonal variations of the error statistics are found to be significant for both the HIRLAM 10m wind speed and the WAM significant wave height. The amplitude of the annual cycle of the bias is about 4 times as large as the average bias of the 10m winds. In the summer months, HIRLAM and WAM show negative bias while it is opposite in the winter months.

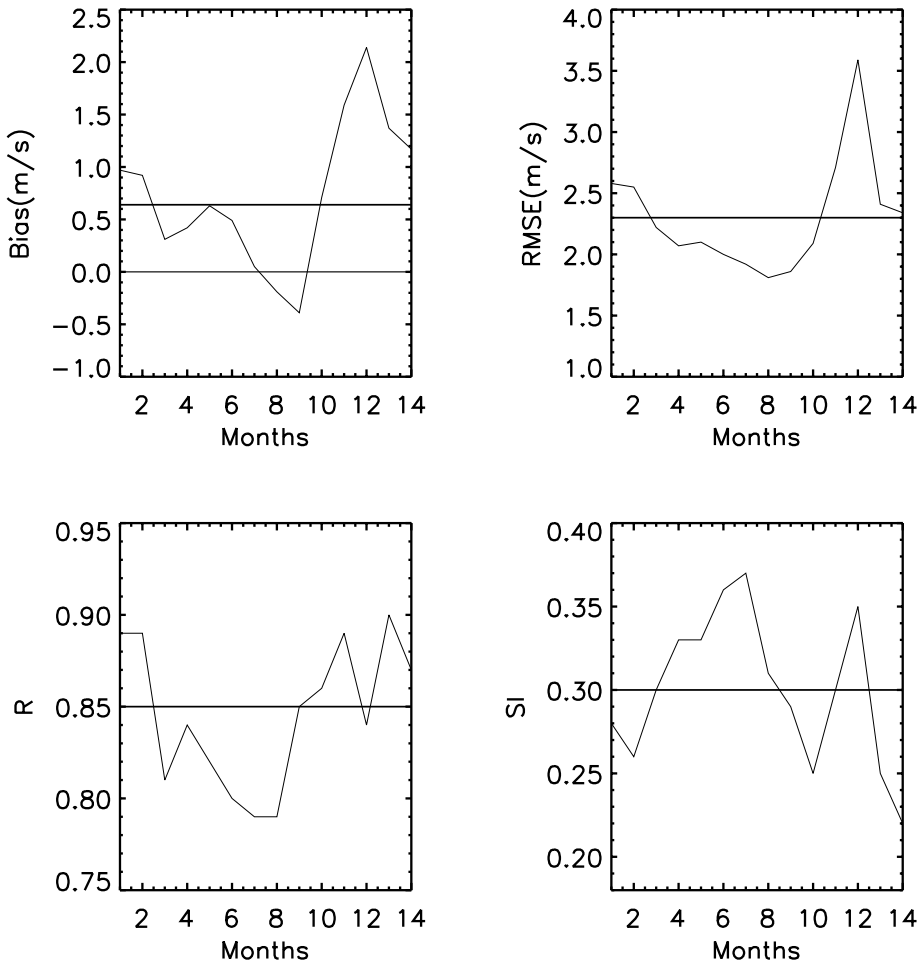

Figure 6: Error statistics of 10m wind speed for 14 months. HIRLAM Bias shown in upper left-panel, Root Mean Square Error in upper-right, correlation coefficient between the model 10m winds and buoy measurements in lower-left and scatter index in lower-right. Mean values are shown as horizontal lines.

The seasonal variation of error statistics of the significant wave height (bias, root-mean-square-error, correlation coefficient between the model and buoy data and scatter index) is shown in Fig.6 for HIRLAM and in Fig. 7 for WAM.

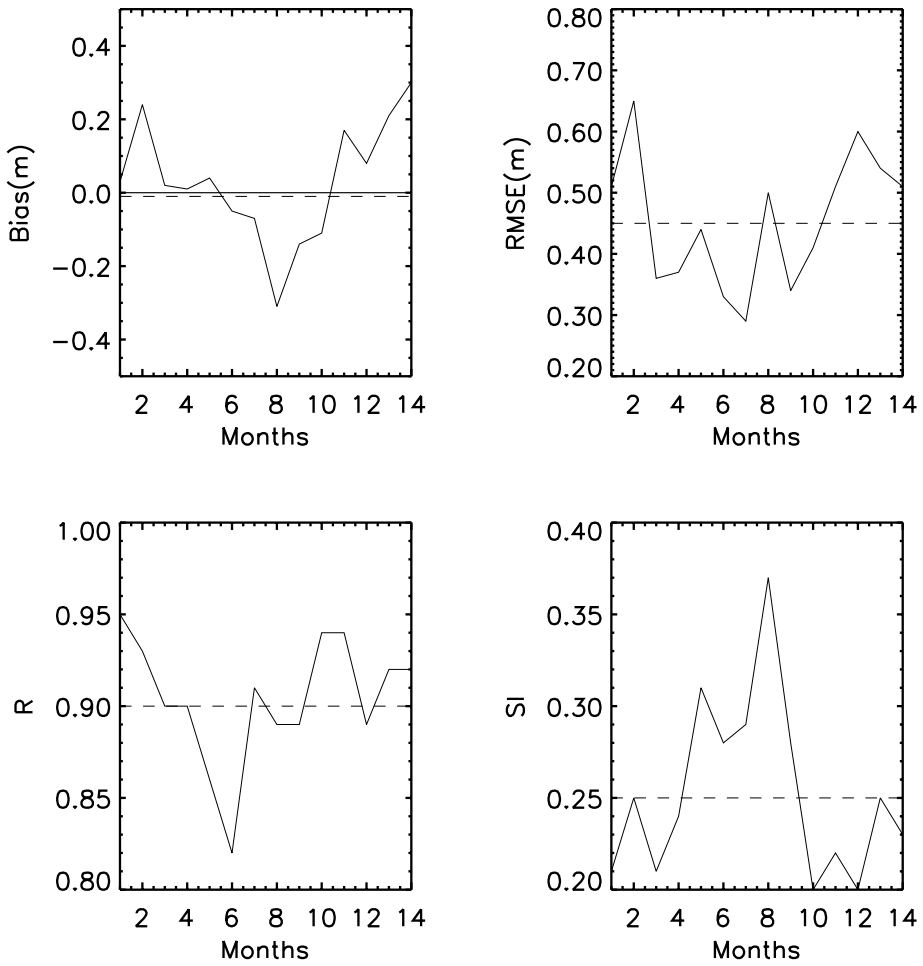

Figure 7: The same as Fig.6 but for the uncoupled WAM significant wave height. Mean values are shown as horizontal lines

2.4.3. Coupled HIRLAM run

In the HIRLAM analysis run, the Charnock number related to sea surface roughness is set to a constant 0.014. Since this value represents a smooth old sea state, the Charnock number from the uncoupled WAM run is normally larger. For a young sea state (with wave age between 5 and 10), the Charnock number can be 5-10 times as large as in the old sea. Fig.8 shows the difference of 10m wind speed and surface stress between the coupled and analysis HIRLAM runs. The wind speed difference has approximately a linear relation with the wind speed. For wind speed less than 5m/s, there is almost no change. This is also related to the special treatment of roughness length when winds are weaker than 5m/s in HIRLAM. In the 5-32 m/s wind range, the coupled HIRLAM winds are decreased by about 3-6%.

For wind speed smaller than 22m/s, the surface stress in the coupled run, however, shows no change. This is because the decreased wind speed and increased roughness length have opposite contributions to the downward momentum flux. For winds larger than 22m/s, the surface stress

in the coupled HIRLAM run shows a slight decrease, which is up to 0.044 Pa at 32m/s wind speed.

A drastic difference happened when the wind speed is larger than 32m/s. There are only a dozen of samples at this high end, all related to the Hurricane on December 3rd 1999. In this case the coupled 10m wind speed is reduced by as much as 4m/s and the surface stress is reduced by over 0.5 Pa. It should be noted that this is just a case study, more investigation is required to quantify the influence of the coupling on the very strong storms.

The 10m wind speed in the coupled HIRLAM run has not been compared with buoy observations. Recognizing that the analysis run has a positive winter bias over 1.0m/s (Fig.7), the reduced wind speed in the coupled runs improves the surface wind simulations.

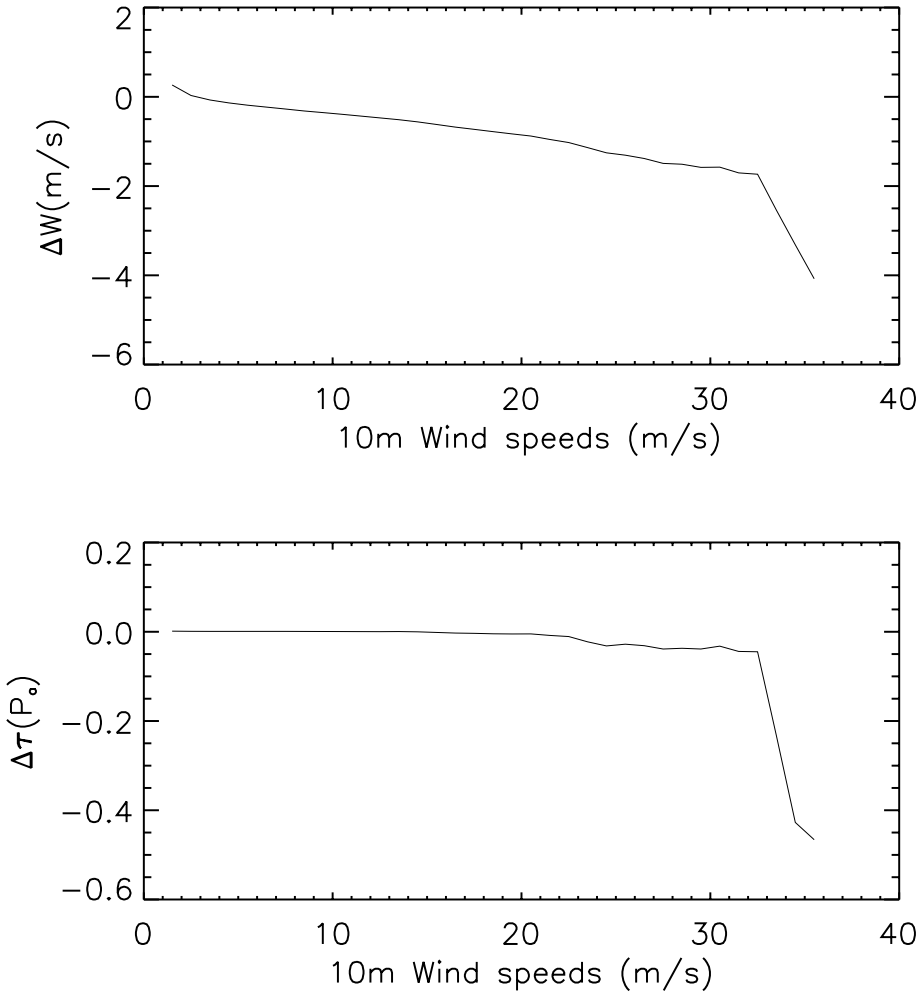

Figure 8: Difference of the 10m wind speed (upper panel) and the surface stress (lower panel) between the coupled and analysis HIRLAM runs.

2.4.4. Coupled WAM run

Due to decreasing winds from the HIRLAM coupled model, the coupled WAM run gives a lower significant wave height than the uncoupled WAM. This compensates the positive bias of the uncoupled WAM (about 0.2m during the same 4-month period, Fig.7). In the case of the Dec. 3rd hurricane, the maximum significant wave height in the coupled run is 2m lower than that in the uncoupled WAM. This suggests that the coupling may have significant influence on waves in the high sea state.

2.4.5. Instant coupling of HIRLAM and WAM

The following experiments were performed with model implemented coupling (see Sec. 2.3.2). Both models were set up to cover the same domain, using identical grid topology, defined on a rotated geographical grid.

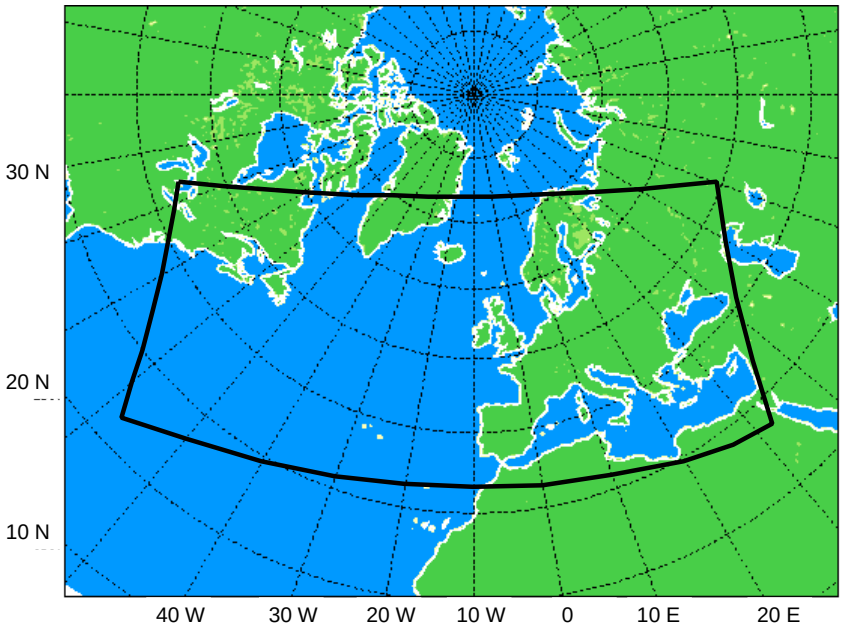

Figure 9: Outline of the model region used in the experiments with instant coupling of HIRLAM and WAM.

The original purpose was a configuration capable for a reanalysis over a longer period over a domain covering Denmark with the surrounding seas. The experiences made during the early studies using the non-instant coupling indicated, however, that it is necessary to include a significantly larger sea area in order to account for the wave processes over the open sea and their influence on the early stage dynamic developments in the above atmosphere. The model domain for the instant coupling studies was therefore enlarged to include the North Sea and even the Northern Atlantic. Fig. 9 shows the model domain, which excludes the polar seas still, because sea-ice treatment is not yet handled in WAM. The domain enlargement required significantly larger computer resources for the simulations, which made it impossible to perform

coupled runs over very long periods. It was therefore decided to concentrate on a one month period instead, and to study the impact of different model and coupling configurations.

The period chosen for the studies covers December 1999, which includes the Danish storm as well as periods with weak winds. A 48 hour hindcast was launched for each day of this period at 0 UTC, using ECMWF analysis to initialize the model. The boundaries were updated with 6 hour frequency using ECMWF global model forecasts. WAM was ”cold started” (see section 2.1.1) with a parameterized wave spectrum at the first day of the period.

Different experiments have been established in order to identify the effect of the instant coupling, as well as to see the impact of the different coupling methods, which the WAM model offers. In addition, different horizontal grid spacings and vertical structures have been used, and a modified vertical diffusion scheme was tested.

A comprehensive overview on the experiments is given in Table 1. The first experiment series addresses the three coupling methods, using 10m wind (V), friction velocity (U) and atmospheric surface stress (T) respectively, as described in Sec. 2.3.1. An uncoupled experiment with a stand-alone HIRLAM has been added for reference. The respective experiment names are added an indicator for the horizontal resolution, where 45 stands for 0.45°, for example.

A second experiment series addresses different vertical structure and vertical diffusion modification. The four coupling experiments of series 1 were performed for a different number of vertical model levels. In addition to the model level structure of 31 vertical levels used in the current operational HIRLAM at DMI, a 40-level model was defined. The level structure of this model was established such that the two lowest model levels were situated at approximately the same heights as the respective wind measurements from the two Eltra wind masts (established by Elsam) at ”Horns Rev” and ”Læsø Syd”. These masts were used for comparisons to the model winds. Table 2 shows the vertical levels of the model atmospheric boundary layer (ABL) for the two model level definitions.

In addition to the vertical level structure, a modified vertical diffusion scheme (Lenderink, 2002) was tested, too. This modified scheme was expected to better describe the wind profile close to the ground. The second series experiments are also listed in Table 1.

In a third series of experiments the horizontal resolution was enhanced to 0.15° grid spacing. The experiment series one and two were, however, not repeated completely in order to limit the immensely growing computer resources necessary to perform the model runs. A reasonable selection from the first two experiment series was identified instead. It was based on the experiences from the two first series and resulted in a small number of experiments with a stand-alone HIRLAM and a coupled HIRLAM-WAM model using friction velocity (see Table 1). The latter choice did not limit the general validity of the results, as will be seen later on. Where the vertical structure is concerned, the 31-level and the 40-level models were also tested in the high resolution setup. These experiments are also listed in Table 1. Experiments with the modified vertical diffusion scheme were not performed with the 0.15°-model, because the verification of the 0.45°-models did not give promising results.

A first validation of the results from the experiments was done for mean sea-level pressure (MSLP) and for the 10m wind. Mean bias and standard deviation over forecast length were determined with respect to the European list of observations of the *European Working Group*

Table 1: Experiment list for the instant coupling studies. See text for a detailed description.

Indicator	hor. grid	Coupling model	vert. levels	vert. diffusion
W45-04-15	0.45°	stand-alone	31	standard
V45-04-15	0.45°	10m wind	31	standard
U45-04-15	0.45°	friction velocity	31	standard
T45-04-15	0.45°	surface stress	31	standard
W45-04-16	0.45°	stand-alone	40	standard
V45-04-16	0.45°	10m wind	40	standard
U45-04-16	0.45°	friction velocity	40	standard
T45-04-16	0.45°	surface stress	40	standard
W45-04-17	0.45°	stand-alone	31	modified
V45-04-17	0.45°	10m wind	31	modified
U45-04-17	0.45°	friction velocity	31	modified
T45-04-17	0.45°	surface stress	31	modified
W45-04-18	0.45°	standalone	40	modified
V45-04-18	0.45°	10m wind	40	modified
U45-04-18	0.45°	friction velocity	40	modified
T45-04-18	0.45°	surface stress	40	modified
W15-05-15	0.15°	stand-alone	31	standard
U15-05-15	0.15°	friction velocity	31	standard
W15-05-16	0.15°	stand-alone	40	standard
U15-05-16	0.15°	friction velocity	40	standard

on Limited Area Modeling (EWGLAM) and with respect to Danish stations (DK). Results for MSLP are given in Figs. 10 to 12.

As can be seen from the figures, the impact on MSLP of coupling HIRLAM and WAM is very small in general. The impact of the vertical structure is stronger. MSLP bias is improved in the 40-level models with respect to the 31-level models (Fig. 10, lower panels). The modification of the vertical diffusion, however, has a negative impact both on MSLP bias and on standard deviation (Fig. 11). The impact of horizontal resolution on the MSLP scores is small. While the bias is slightly larger in the 0.15° models than in the 0.45° models, standard deviation is slightly better (Fig. 10 and 12).

The statistics for 10m wind are given in Figs. 13 to 18. The main differences show up between the uncoupled HIRLAM and the coupled HIRLAM-WAM simulations, especially for the Danish station list (DK), which contains more coastal stations than the EWGLAM list. The coupled runs systematically score better. This improvement can be equally found in the 0.45°-models and in the 0.15° models. The standard deviation improves to a small amount with increasing horizontal resolution (compare Figs. 13 and 17, or 14 and 18, respectively). This improvement

Table 2: Vertical level structures of the model ABL used in the instant coupling studies. The 31-level model coincides with the operational HIRLAM at DMI.

31-level model		40-level model	
level	height in m	level	height in m
23	1548.7	27	1561.5
24	1202.4	28	1310.1
25	907.2	29	1083.4
26	659.6	30	886.3
27	458.5	31	710.0
28	301.9	32	560.5
29	183.9	33	437.4
30	103.5	34	327.7
31	31.7	35	241.0
		36	172.3
		37	116.5
		38	77.3
		39	45.5
		40	15.0

is more pronounced when regarding the Danish stations.

There is no significant difference in 10m wind scores between the different coupling methods, which may indicate that the unified treatment of the atmospheric input into WAM has more impact on the model than the choice of the atmospheric parameter.

In a second validation comparison with wind observations at the two Eltra (Elsam) wind masts at ”Horns Rev” and ”Læsø Syd” were performed. As can be seen from Table 2, the lowest model level of the 31-level models almost coincides with the height of the 30m measurements from the wind masts. In the 40-level models, the two lowest model levels coincide with the measurement heights at 15m and 45m, respectively. The model data from these levels were therefore compared to the respective measurements.

The wind observations from the meteorological masts are available as 10 minute averages. As the model field data refers to 15 minute averages and was written with 1 hour frequency, comparison was made to the measurements referring to the 10 minute average for the full hour. A comparison of the model data to a ”20 Minute average” determined from the two 10 minute averages at the full hour and at 10 minutes shows that the results of the verification are generally independent from this choice.

Again bias and standard deviation between model and observation were determined. However, only the coupling model using friction velocity (U45/U15) has been included in the comparisons, because there is no significant difference between the results from the different coupling models.

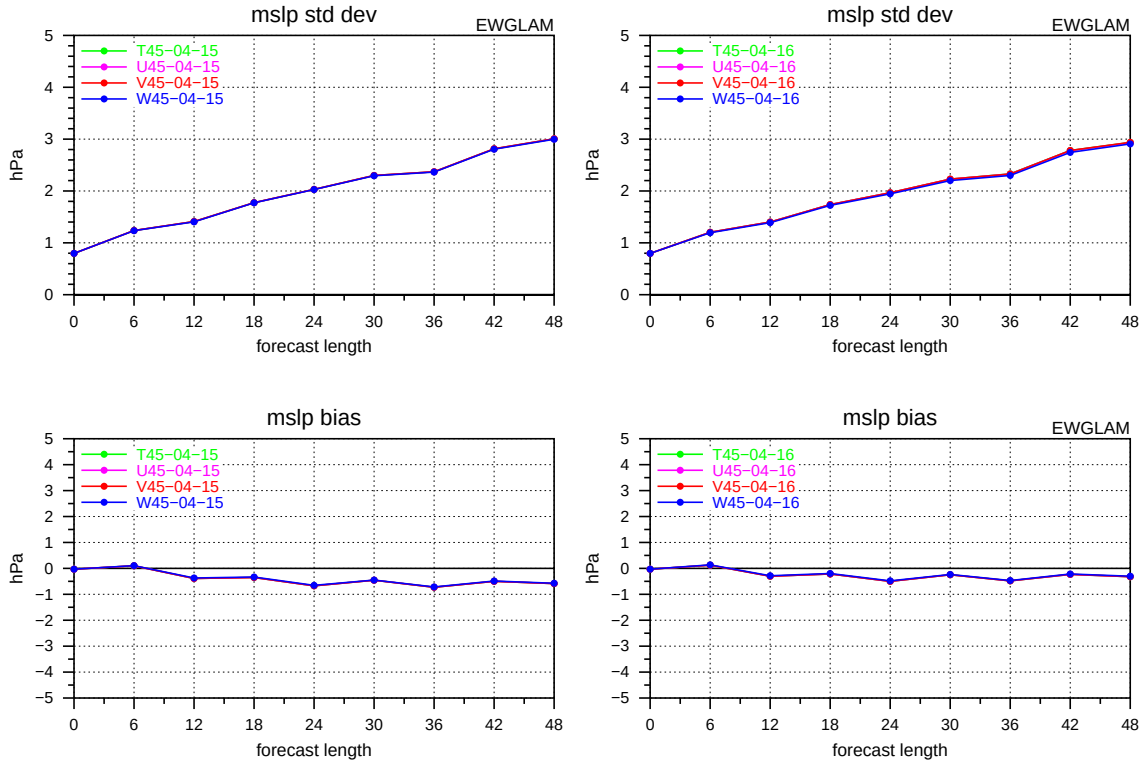

Figure 10: Bias (lower panels) and standard deviation (upper panels) for MSLP of the 0.45 °-models verified against the EWGLAM stations. The left panels refer to the 31-level models, and the right panels to the 40-level models, using standard vertical diffusion respectively. See Table 1 for reference of the experiment names.

Fig. 19 shows the results for the 30m wind. As for the 10m wind, the coupling between HIRLAM and WAM generally diminishes the wind speed, which becomes immediately clear when looking at the biases (lower panels in Fig. 19). The colours in the panels of the figure are as follows:

colour	model
light blue	0.45 °-model with standard vertical diffusion, standalone
dark blue	0.45 °-model with standard vertical diffusion, coupled
grey	0.45 °-model with modified vertical diffusion, standalone
green	0.45 °-model with modified vertical diffusion, coupled
magenta	0.15 °-model with standard vertical diffusion, standalone
red	0.15 °-model with standard vertical diffusion, coupled

The same colour codes have been used for the results from the 40-level models, i. e. for 15m wind (Fig. 20) and for 45m wind (Fig. 21).

As the experiments only comprise one month, and hindcasts were launched at 0 UTC, the diurnal cycle is retained and shows up especially at ”Horns Rev”. A reason for this is that the wind

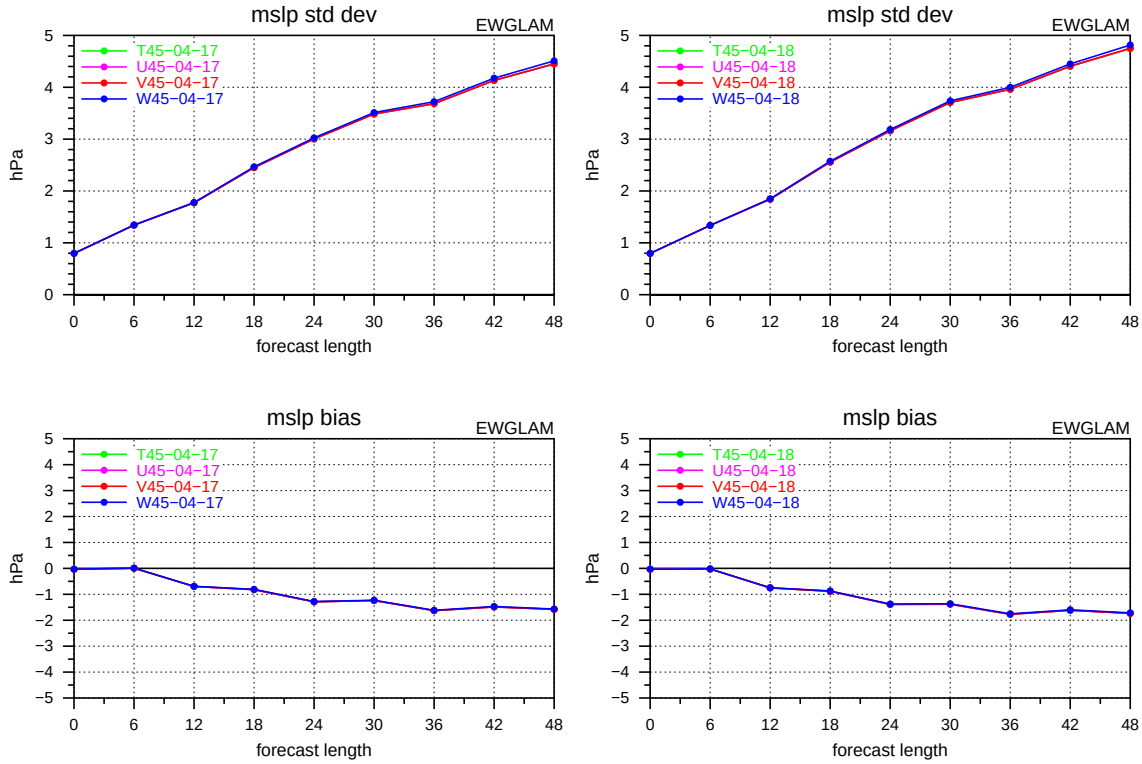

Figure 11: Bias (lower panels) and standard deviation (upper panels) for MSLP of the 0.45 °-models verified against the EWGLAM stations. The left panels refer to the 31-level models, and the right panels to the 40-level models, using modified vertical diffusion respectively. See Table 1 for reference of the experiment names.

measurements at ”Horns Rev” where not available between 4^{th} and 14^{th} December, which reduced the sample size considerably.

There is a positive bias in the winds of the lowest model level, which are the 30m wind (31-level models) and the 15m winds (40-level models), in all models with standard vertical diffusion (blue and red curves in Fig 19 and 20). In the 40-level models, the next model level wind (45m wind, see Fig. 21) shows a reduced positive bias or becomes even negative. This indicates that the representation of the vertical wind profile is too flat towards the ground, resulting in an overestimation of wind speed near the ground.

The models with modified vertical diffusion, however, seem to represent the low level vertical wind profile much better. The bias between the 15m wind and the 45m wind remains approximately the same, especially at ”Læsø Syd” (Figs. 20 and 21, lower right panel), where the verification is based on a larger data amount.

It is actually not possible to draw a general conclusion concerning the performance of the coupled and uncoupled model on the one hand, and the performance of the 0.45 °-model and the 0.15 °-model on the other hand with respect to bias. This is because the representation of the vertical profile, which is strongly influenced by the vertical diffusion, has a much larger impact than the coupling, the horizontal resolution, or the vertical level distribution.

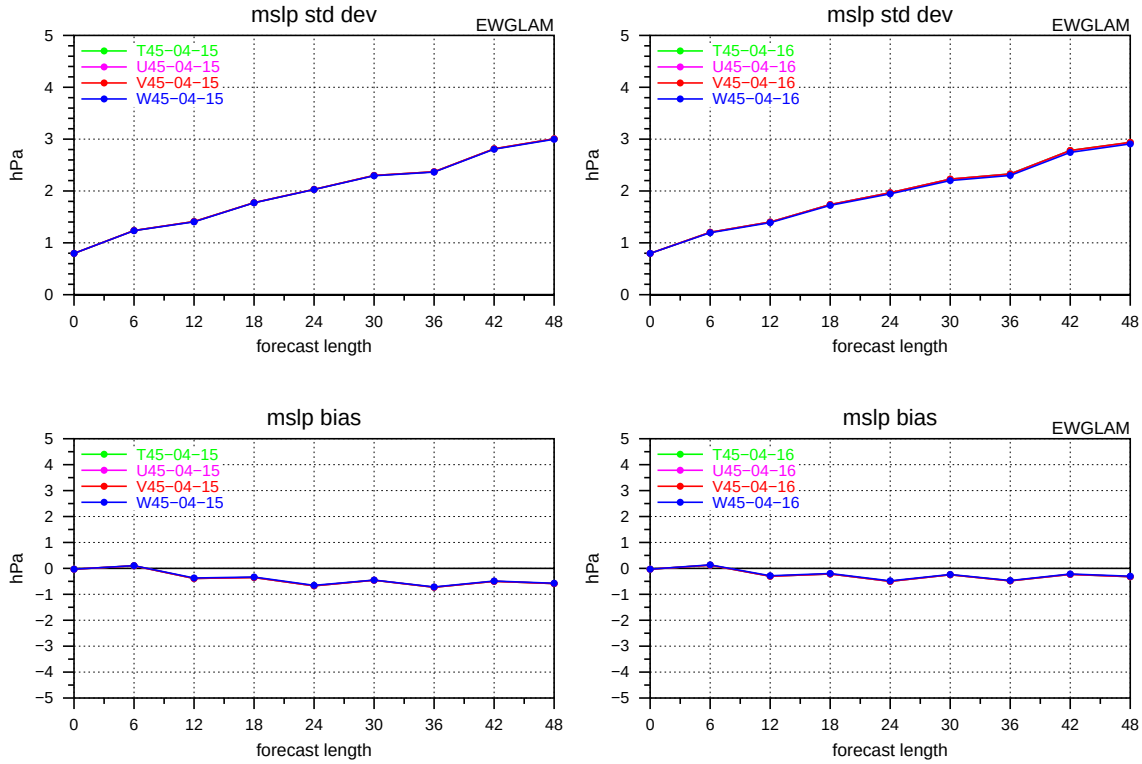

Figure 12: Bias (lower panels) and standard deviation (upper panels) for MSLP of the 0.15 °-models verified against the EWGLAM stations. The left panels refer to the 31-level models, and the right panels to the 40-level models, using standard vertical diffusion respectively. See Table 1 for reference of the experiment names.

The differences in the standard deviation between the different models are generally small, but the coupled 0.15 °-model with standard vertical diffusion (red curves in Figs. 19, 20 and 21) has the best overall performance. The largest errors mainly occur in the model runs with modified vertical diffusion (grey and green curves). This becomes especially clear at the ”Læsø Syd” wind mast.

With respect to wind energy use, it is of interest, how the models perform in forecasting those wind speeds, which wind turbines usually are capable of exploiting. The wind speed range begins for most wind turbines around 3–4m/s and ends at around 25m/s. Another verification has therefore been carried out, which bins the comparison in velocity ranges of the observed wind speed. These ranges have been chosen to 0–5m/s, 5–10m/s, 10–15m/s, 15–20m/s and 20–25m/s. Figs. 22 – 24 show the verification scores for these ranges. The colour codes are the same as in the previous figures. Where the bias of the forecast error is concerned, the general picture again shows that there is a poisitive bias in the models with standard vertical diffusion, For large wind speeds, however, this bias often is reduced or even becomes negative.

Again the finding from above is confirmed that the coupling of HIRLAM and WAM reduces wind speeds and has impact on the bias regardless of the sign of the bias, and standard deviation tends to be reduced through the coupling. There is, however, one exception, which can be seen in the 0–5m/s velocity bin. The coupling has no significant influence on the predicion of these

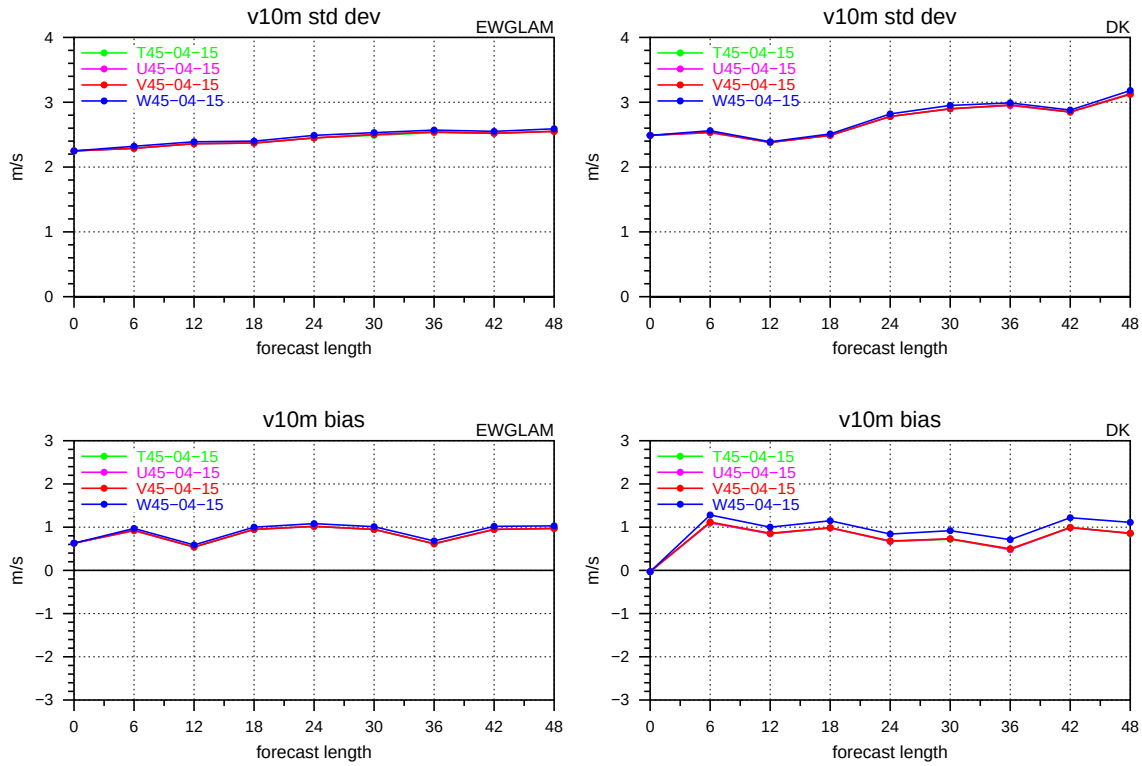

Figure 13: Bias (lower panels) and standard deviation (upper panels) for 10m wind of the 0.45 °-models with 31 levels and standard vertical diffusion verified against the EWGLAM stations (left panels) and against the Danish stations (right panels). See Table 1 for reference of the experiment names.

low wind speeds, and this is due to the transition treatment of the sea surface roughness (Eqs. 6 and 7).

The general behaviour of the standard deviation over the velocity bins is rather flat, so even though the data volume is not large, it may be concluded that the absolute error does not increase significantly with increasing wind speed. Contrary to the positive effect of the coupling on the error, the increase in horizontal resolution does not generally lead to a reduction of the error. It is often the wind speeds beyond 15m/s, where an improvement through higher horizontal resolution can be detected.

The relative change of the forecast error in the wind speed range exploited by wind turbines can be assessed from Figs. 25 to 27, which show the relative error with respect to wind speed. It is largest for the small wind speeds and decreases most often with growing wind speed, especially at ”Læsø Syd” (right panels in Figs. 25, 26 and 27). The figures indicate a small improvement in the wind speed when coupling HIRLAM and WAM and when increasing horizontal resolution. This has been summarized in Table 3. It shows that coupling HIRLAM and WAM improves the wind speed forecast about 1%, where most improvement is accomplished in the wind speed ranges between 5–10m/s and 10-15m/s, and the improvement is more pronounced in the high resolution model. As the power curves of wind turbines usually have steepest ascent

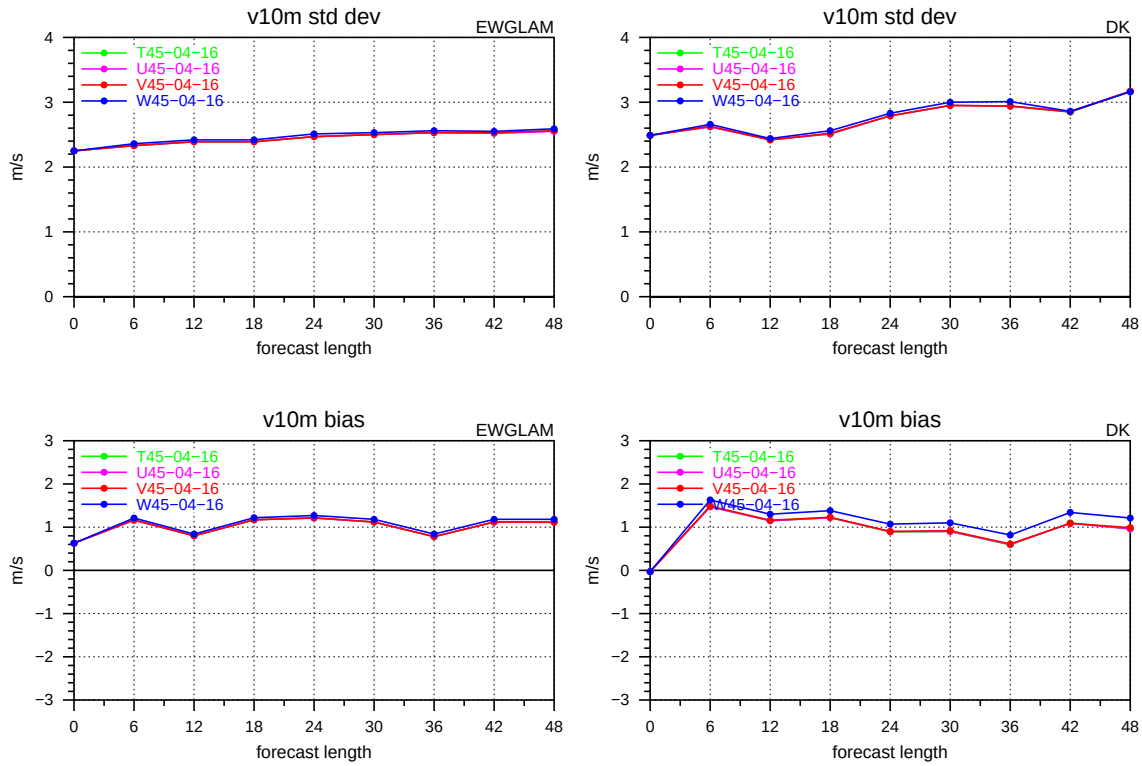

Figure 14: Bias (lower panels) and standard deviation (upper panels) for 10m wind of the 0.45 °-models with 40 levels and standard vertical diffusion verified against the EWGLAM stations (left panels) and against the Danish stations (right panels). See Table 1 for reference of the experiment names.

at wind speeds between 5 and 15m/s, the effect of coupling on the improvement of wind power prediction may be expected to be somewhat higher.

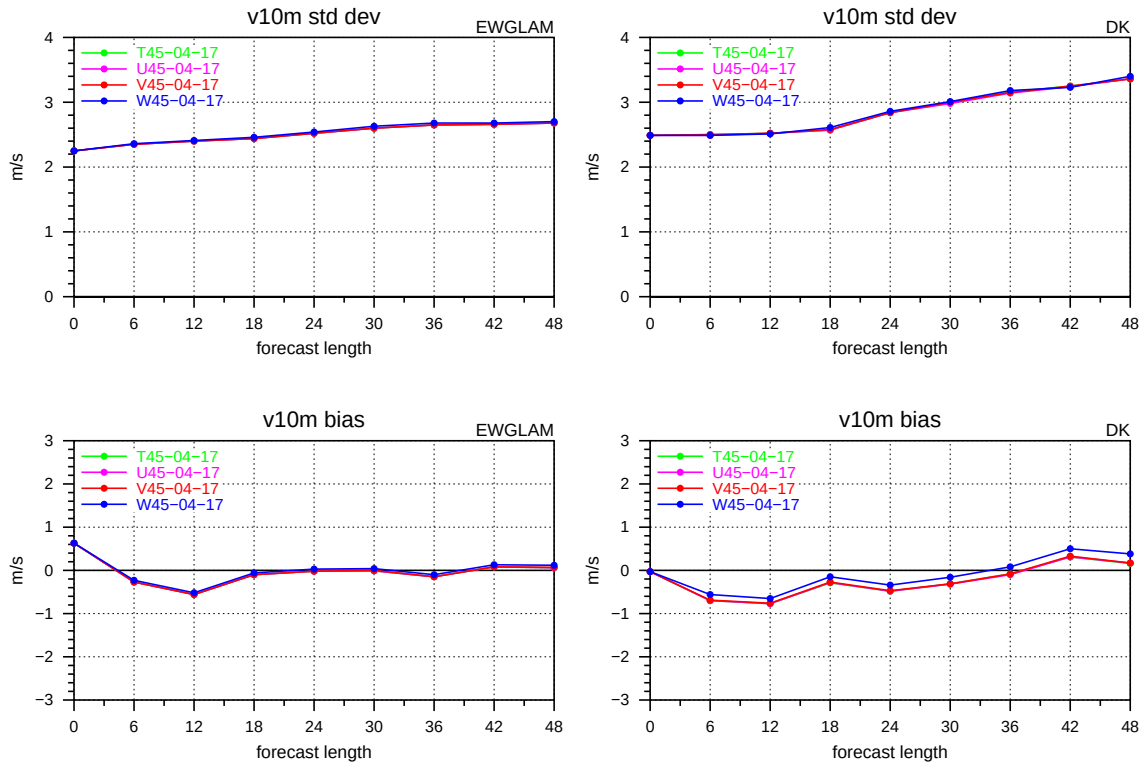

Figure 15: Bias (lower panels) and standard deviation (upper panels) for 10m wind of the 0.45 °-models with 31 levels and modified vertical diffusion verified against the EWGLAM stations (left panels) and against the Danish stations (right panels). See Table 1 for reference of the experiment names.

The improvement of wind speed forecasts when increasing horizontal resolution from 0.45 ° to 0.15 ° is not as clear as in the case of coupling HIRLAM and WAM. As Table 3 shows, there is even a deterioration in the range of the small wind speeds. This is less significant in the coupled HIRLAM-WAM models. The most significant improvement is in the range of 15-20 m/s, both independent of whether HIRLAM runs as standalone or coupled to WAM.

In addition to the verification scores, the experiments are evaluated on basis of a case study. The behaviour of the models outlined in Table 1 is regarded for the Danish storm on December 3rd 1999. Figs. 28 and 29 show the 30m wind speed at ”Horns Rev” and at ”Læsø Syd”, respectively, during December 2nd and 4th, and Figs. 30 and 31 show the time series shifted one day. The colour curves refer to the models as above. Differences between standalone HIRLAM and coupled HIRLAM and WAM show up at some points, the most remarkable of which is at ”Læsø Syd” after December 3rd 21:00 in the simulations started at December 3rd 0 UTC (Fig. 31), where the model wind of the 0.15 ° coupled model (red curve) increases significantly earlier than in the standalone HIRLAM (magenta curve).

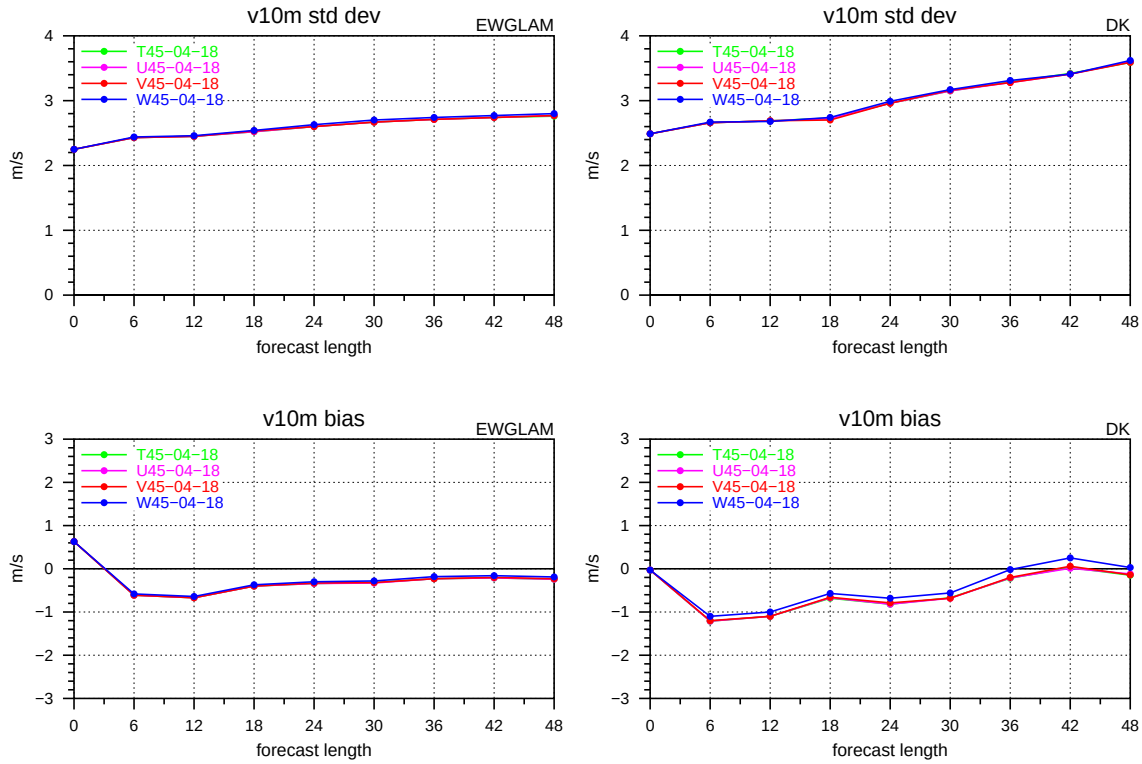

Figure 16: Bias (lower panels) and standard deviation (upper panels) for 10m wind of the 0.45 °-models with 40 levels and modified vertical diffusion verified against the EWGLAM stations (left panels) and against the Danish stations (right panels). See Table 1 for reference of the experiment names.

Table 3: Average improvement of the relative forecast error in % for wind speed over the two locations ”Horns Rev” and ”Læsø Syd”, when coupling HIRLAM and WAM (I), and when increasing horizontal resolution from 0.45 ° to 0.15 ° (II). Numbers are separated for the 0.45 °/0.15 ° models and the stand-alone/coupled models, respectively.

comparison		model	5–10 m/s	10–15 m/s	15–20 m/s	20–25 m/s
I	stand-alone – coupled	0.45 °	-0.87	0.86	1.29	0.89
		0.15 °	0.96	1.20	1.12	0.42
II	0.45 ° – 0.15 °	standalone	-1.96	-0.21	2.83	0.48
		coupled	-0.73	0.08	2.66	0.01

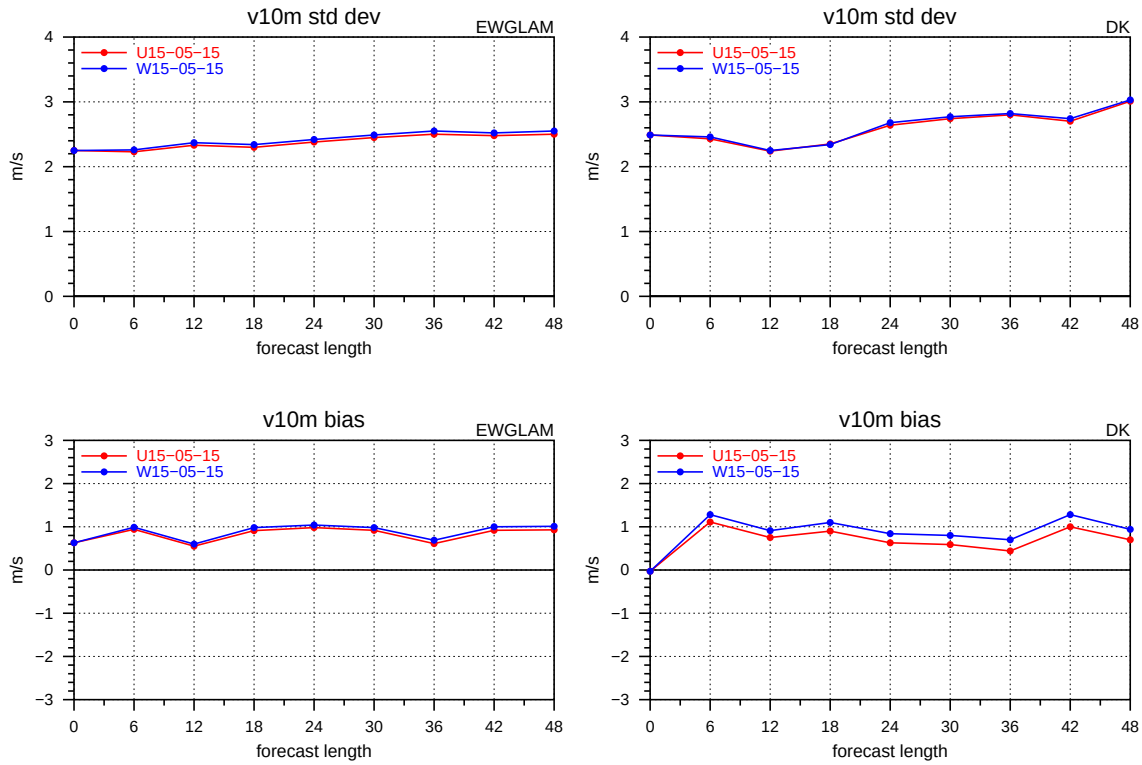

Figure 17: Bias (lower panels) and standard deviation (upper panels) for 10m wind of the 0.15 °-models with 31 levels verified against the EWGLAM stations (left panels) and against the Danish stations (right panels). See Table 1 for reference of the experiment names.

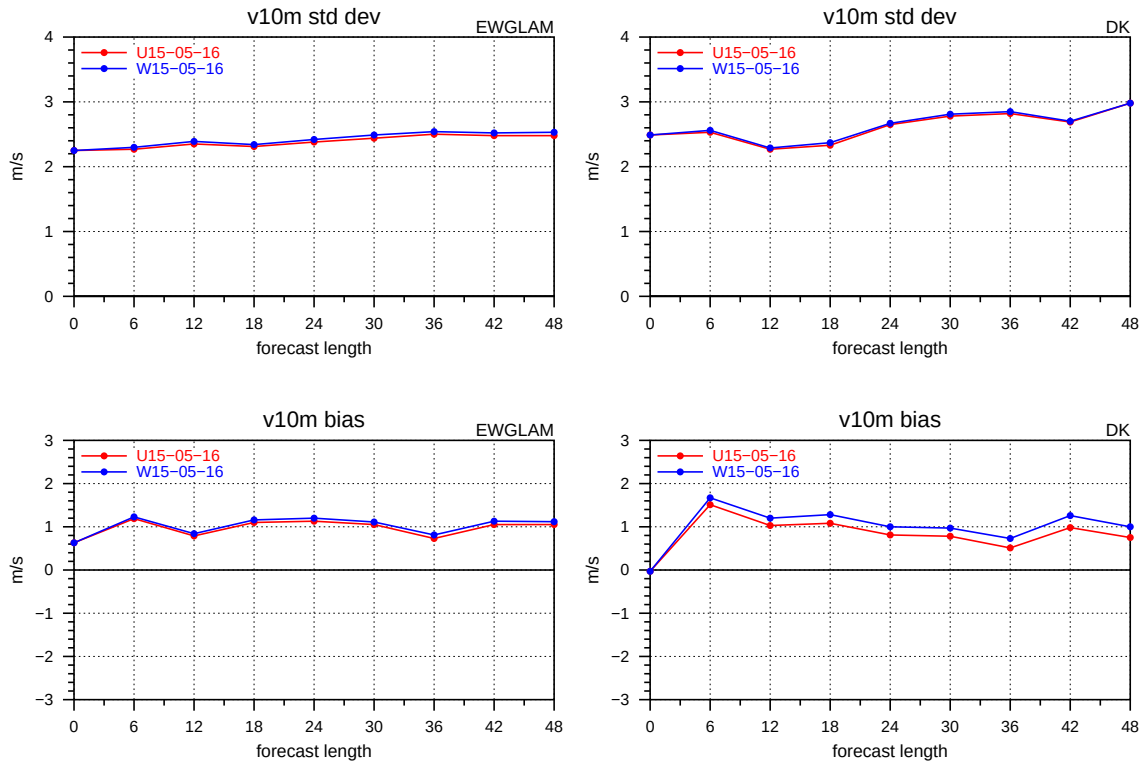

Figure 18: Bias (lower panels) and standard deviation (upper panels) for 10m wind of the 0.15 °-models with 40 levels verified against the EWGLAM stations (left panels) and against the Danish stations (right panels). See Table 1 for reference of the experiment names.

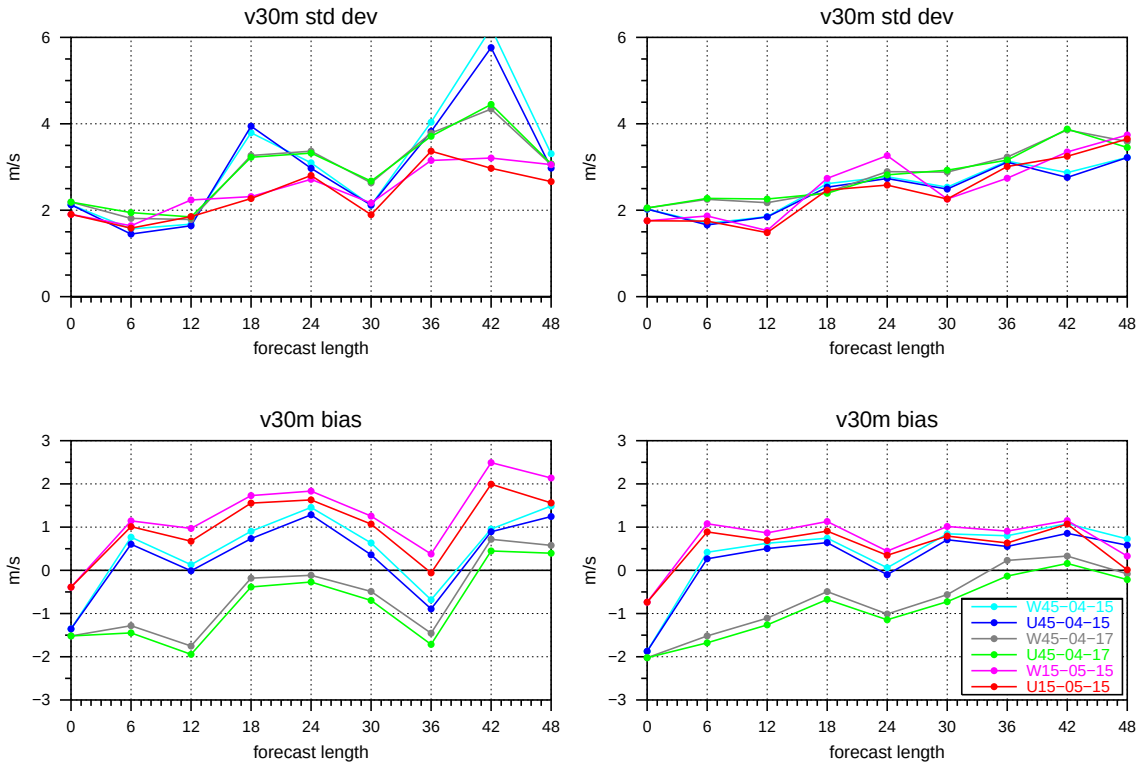

Figure 19: Bias (lower panels) and standard deviation (upper panels) for 30m wind of selected models verified against the wind masts ”Horns Rev” (left panels) and ”Læsø Syd” (right panels). See Table 1 for reference of the experiment names.

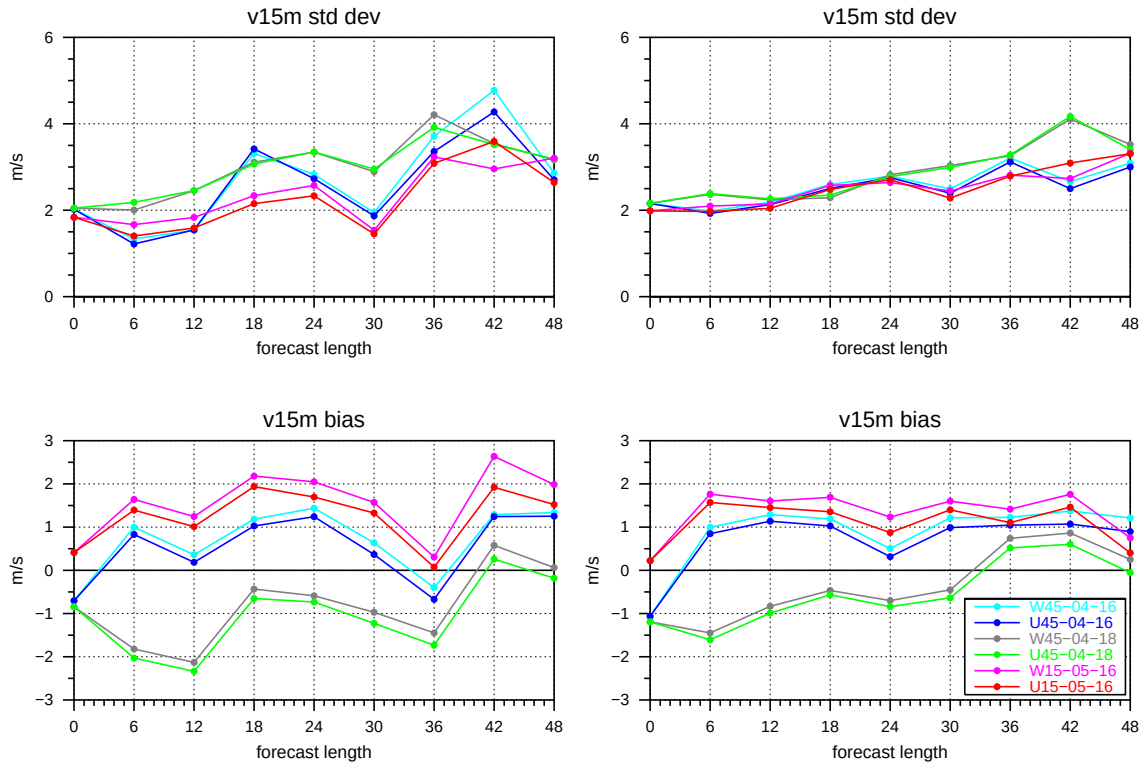

Figure 20: Bias (lower panels) and standard deviation (upper panels) for 15m wind of selected models verified against the wind masts ”Horns Rev” (left panels) and ”Læsø Syd” (right panels). See Table 1 for reference of the experiment names.

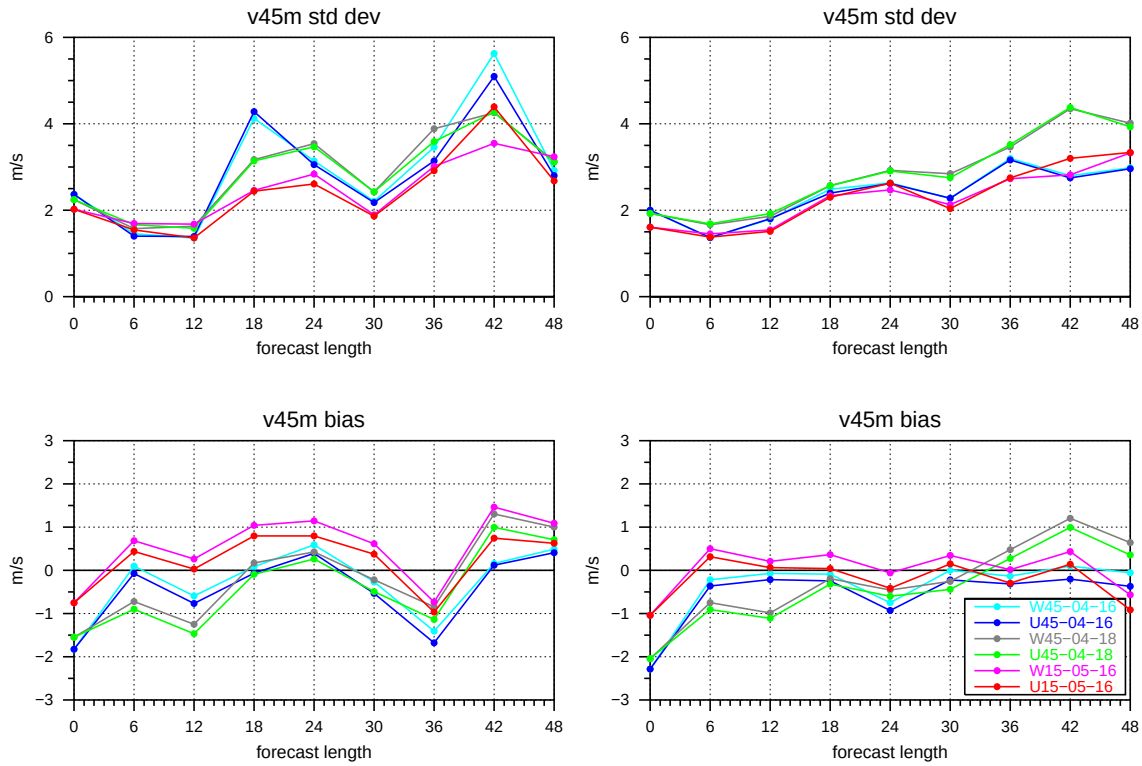

Figure 21: Bias (lower panels) and standard deviation (upper panels) for 45m wind of selected models verified against the wind masts ”Horns Rev” (left panels) and ”Læsø Syd” (right panels). See Table 1 for reference of the experiment names.

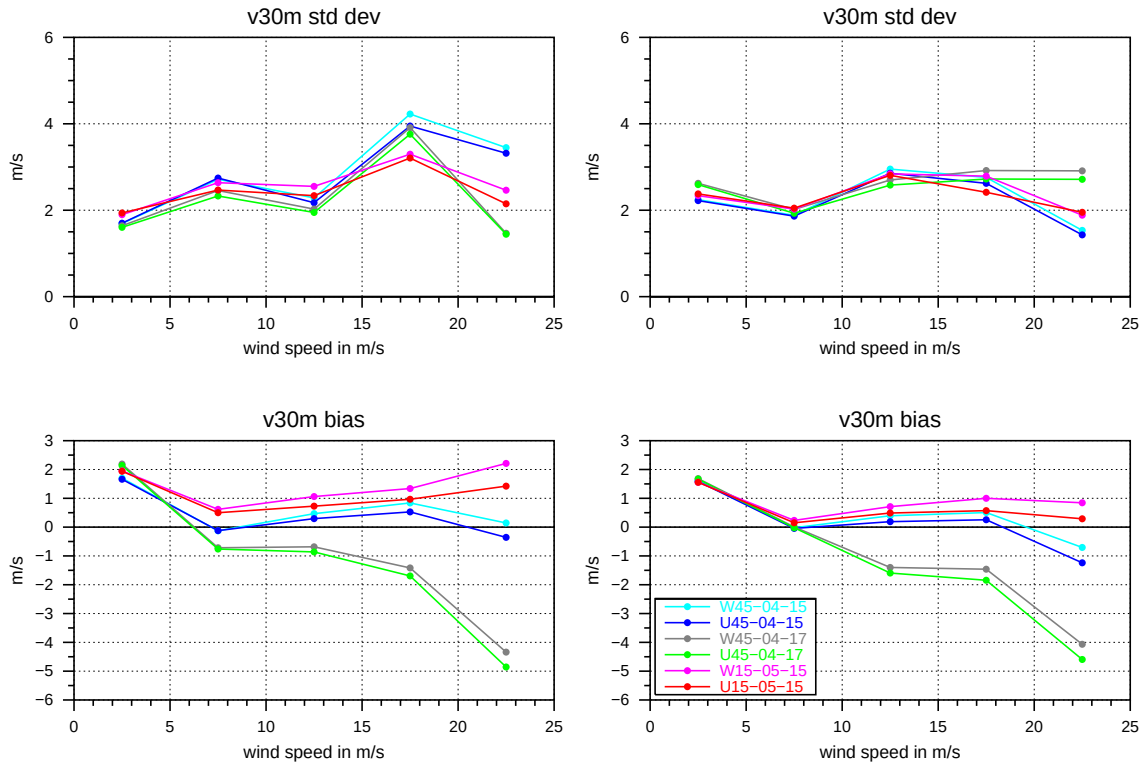

Figure 22: Bias (lower panels) and standard deviation (upper panels) over wind speeds relevant for wind turbines for 30m wind of selected models verified against the wind masts ”Horns Rev” (left panels) and ”Læsø Syd” (right panels). See Table 1 for reference of the experiment names.

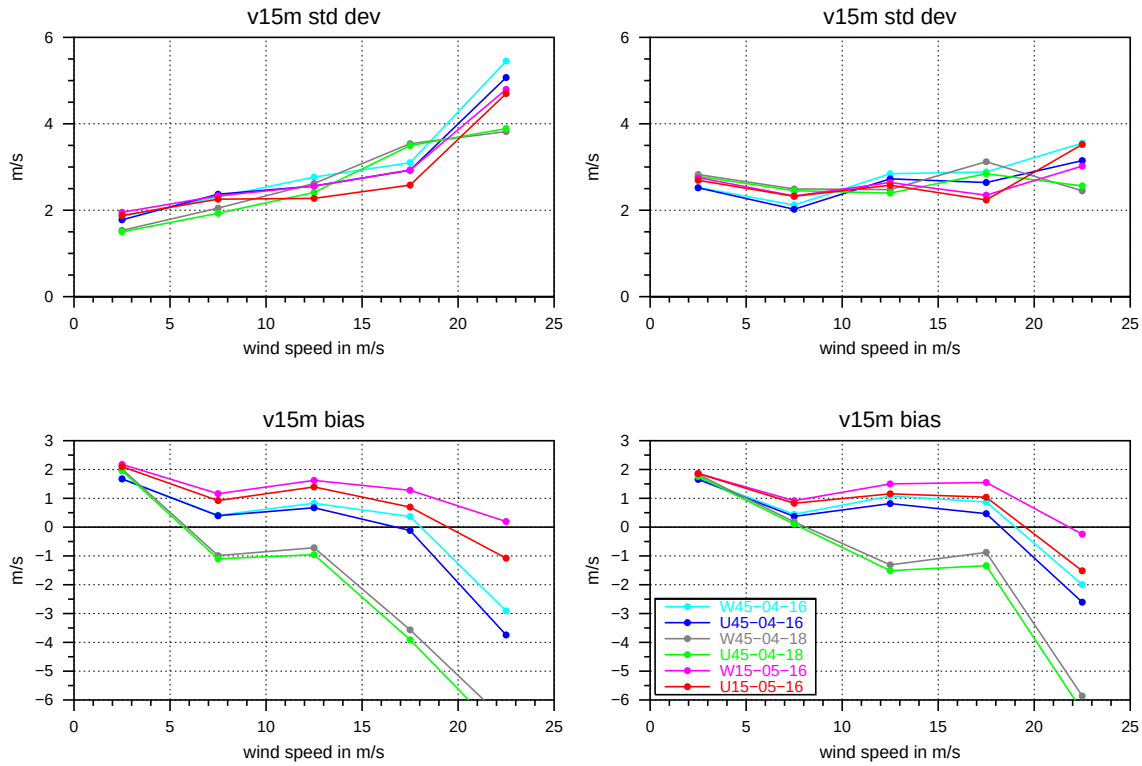

Figure 23: Bias (lower panels) and standard deviation (upper panels) over wind speeds relevant for wind turbines for 15m wind of selected models verified against the wind masts ”Horns Rev” (left panels) and ”Læsø Syd” (right panels). See Table 1 for reference of the experiment names.

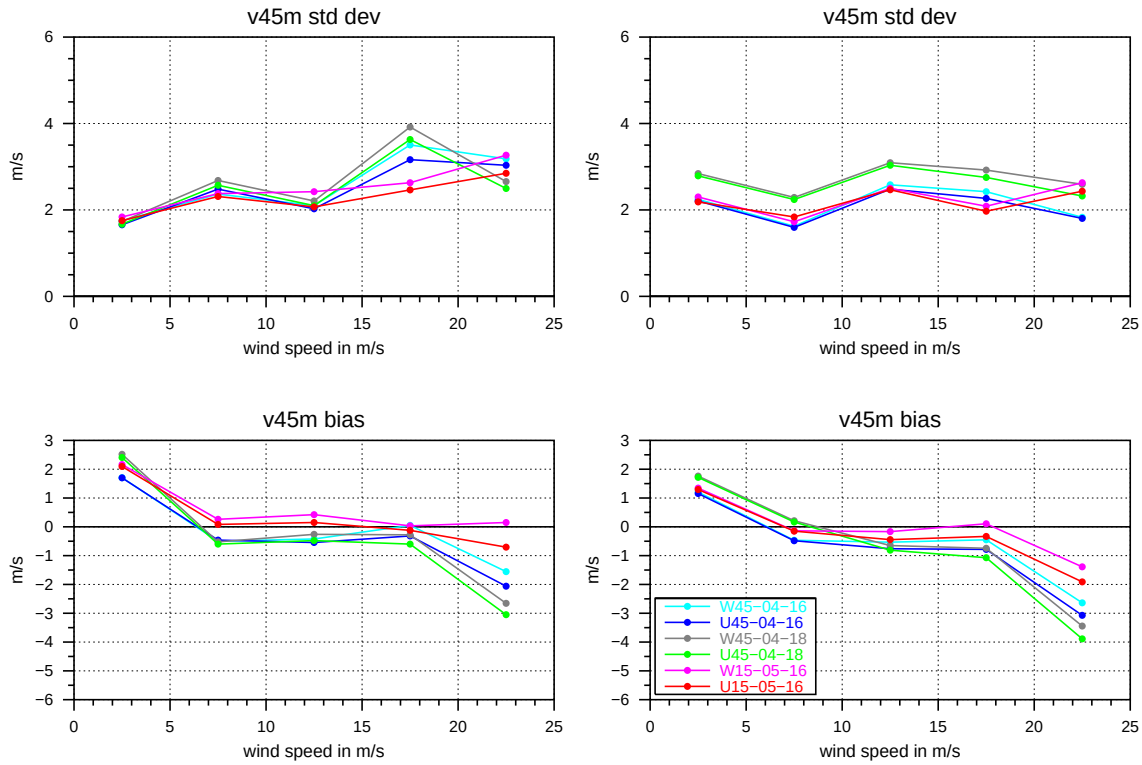

Figure 24: Bias (lower panels) and standard deviation (upper panels) over wind speeds relevant for wind turbines for 45m wind of selected models verified against the wind masts ”Horns Rev” (left panels) and ”Læsø Syd” (right panels). See Table 1 for reference of the experiment names.

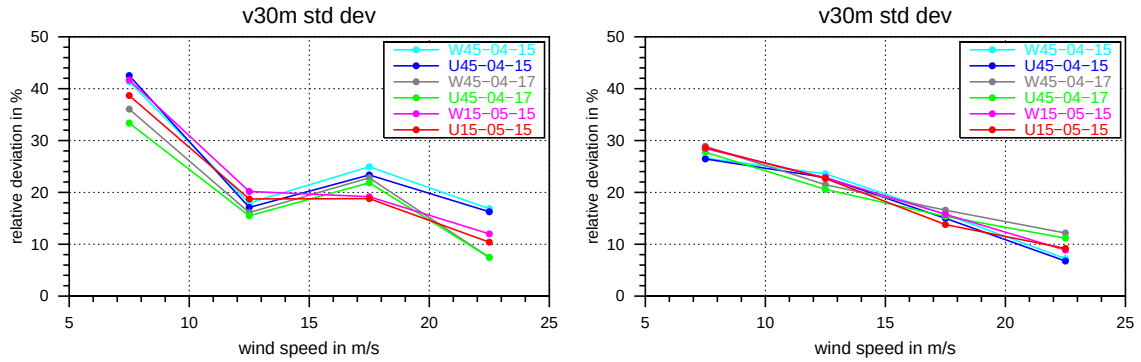

Figure 25: Relative error over wind speeds relevant for wind turbines for 30m wind of selected models verified against the wind masts ”Horns Rev” (left panels) and ”Læsø Syd” (right panels). See Table 1 for reference of the experiment names.

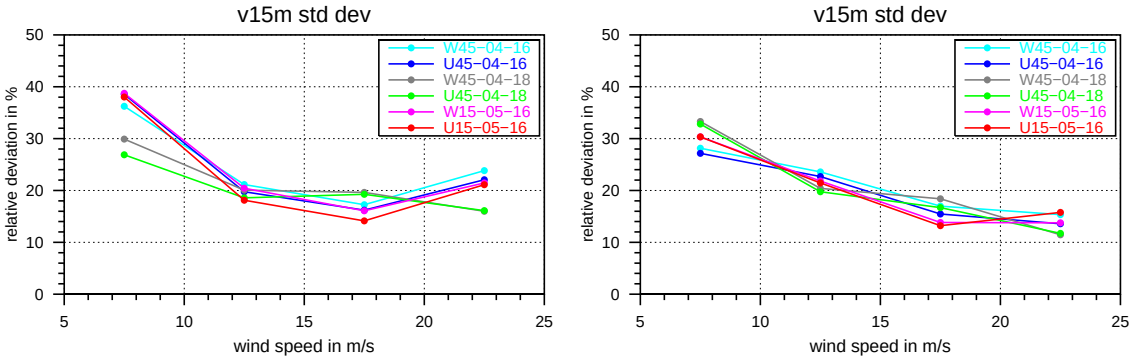

Figure 26: Relative error over wind speeds relevant for wind turbines for 15m wind of selected models verified against the wind masts ”Horns Rev” (left panels) and ”Læsø Syd” (right panels). See Table 1 for reference of the experiment names.

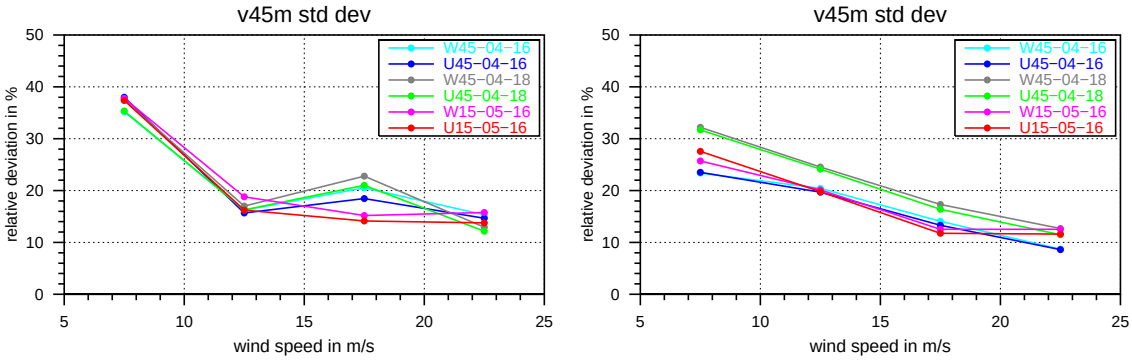

Figure 27: Relative error over wind speeds relevant for wind turbines for 45m wind of selected models verified against the wind masts ”Horns Rev” (left panels) and ”Læsø Syd” (right panels). See Table 1 for reference of the experiment names.

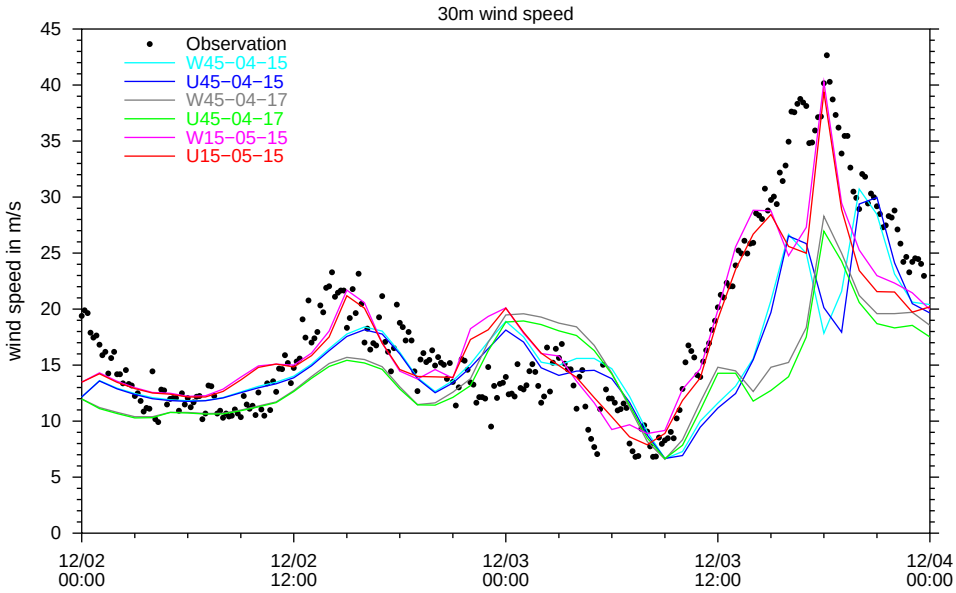

Figure 28: Temporal course of the wind speed observation at 30m height between 2$^{\mathrm{nd}}$ and 4$^{\mathrm{th}}$ December 1999 at "Horns Rev", and, in colours, the simulations of 30m wind from different models (Table 1) of the 31-level set, started at 2$^{\mathrm{nd}}$ December.

The best correlation between model and measurement as a whole in the case of the December 1999 storm seems to be the coupled 0.15°-model (red curves in Figs. 28 to 31). The most significant improvement through this model can be seen at "Horns Rev" during the culmination of the storm between in the second half of December 3$^{\mathrm{rd}}$. Only the 0.15° models capture the wind speed peak, and in the simulation started at December 3$^{\mathrm{rd}}$ (Fig. 30) the coupled model fits the observation best. Using high horizontal resolution is decisive in this case.

The results from the 40-level models for this case (not shown) are very similar to the results from the 31-level models, and the positive impact of horizontal resolution is also present in these simulations.

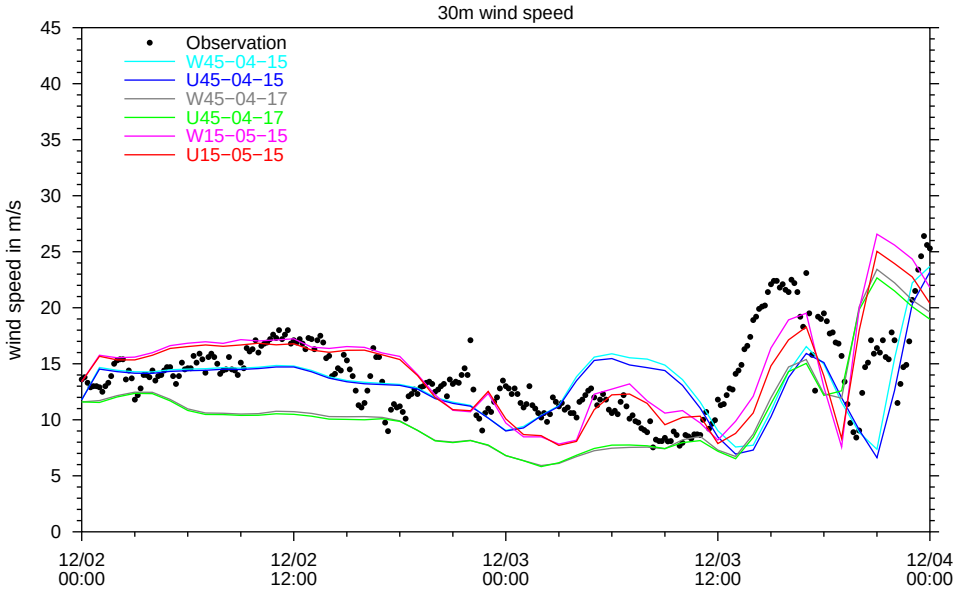

Figure 29: Temporal course of the wind speed observation at 30m height between 2$^{\mathrm{nd}}$ and 4$^{\mathrm{th}}$ December 1999 at ”Læsø Syd”, and, in colours, the simulations of 30m wind from different models (Table 1) of the 31-level set, started at 2$^{\mathrm{nd}}$ December.

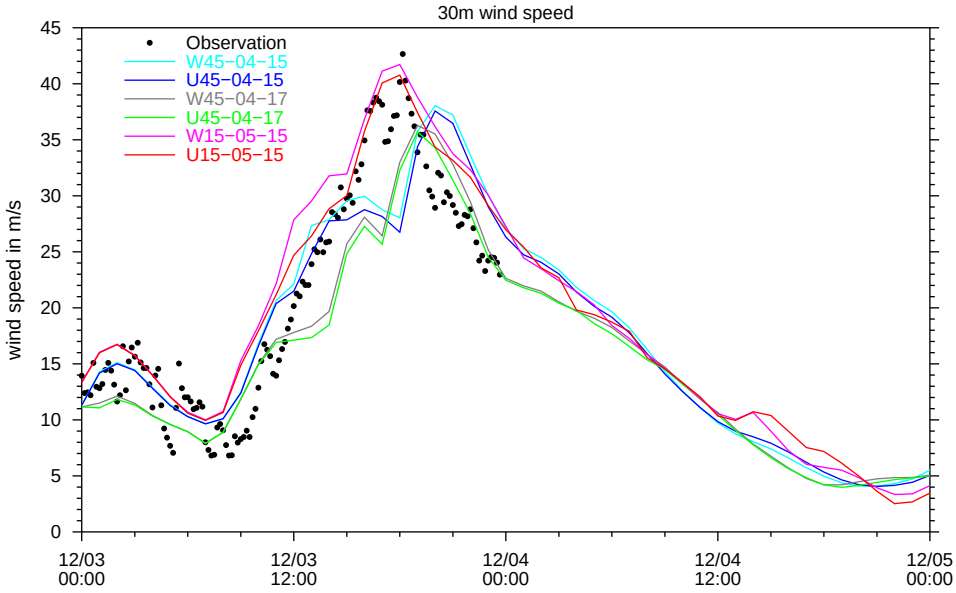

Figure 30: Temporal course of the wind speed observation at 30m height between 3$^{\mathrm{rd}}$ and 5$^{\mathrm{th}}$ December 1999 at ”Horns Rev”, and, in colours, the simulations of 30m wind from different models (Table 1) of the 31-level set, started at 3$^{\mathrm{rd}}$ December.

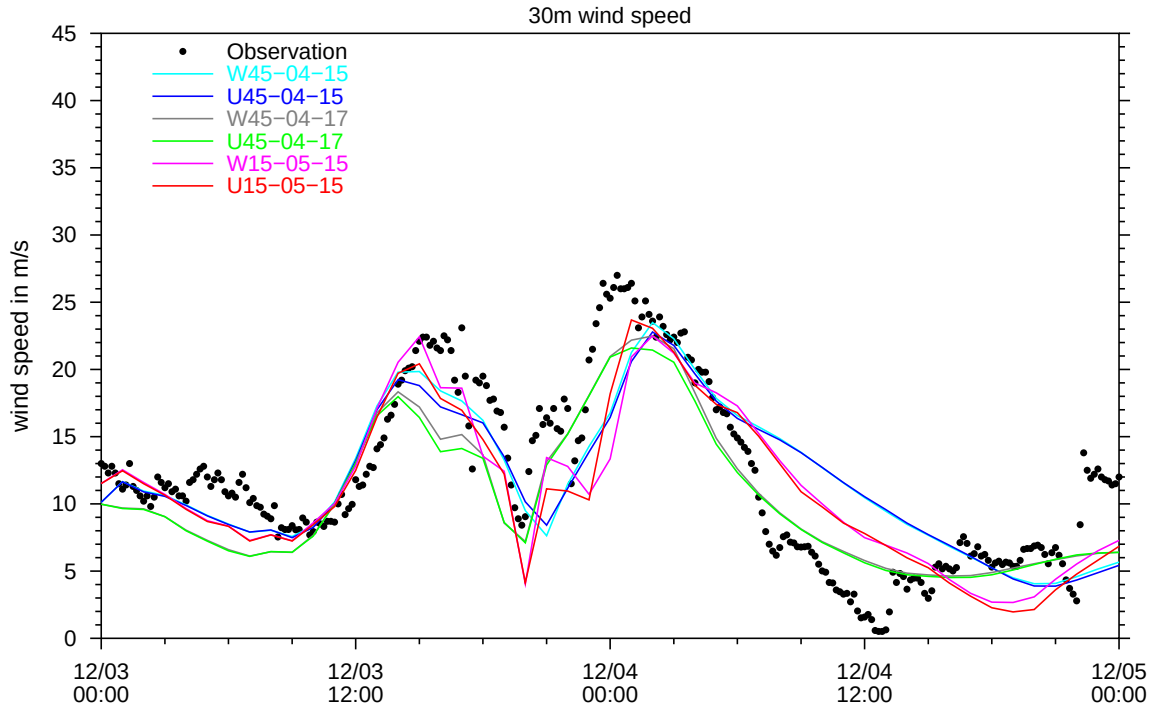

Figure 31: Temporal course of the wind speed observation at 30m height between 3^{rd} and 5^{th} December 1999 at "Læsø Syd", and, in colours, the simulations of 30m wind from different models (Table 1) of the 31-level set, started at 3^{rd} December.

3. Wind forecasting over land

Forecasting the wind or more specifically the wind resource over land has been done for many years. With the growth of exploitation of wind energy it has become more and more important. Any analysis of the economy of wind farms shows that by far the most important parameter is the mean wind speed at the site (see e.g. (Hansen and Tande, 1993)).

Models for deriving the wind resource at a site are many, but one of the first more systematic approaches to this field was the "Wind Atlas for Denmark" (Petersen et al., 1981), where the wind resource for any place in Denmark was derived from the synoptic pressure field. After that, the *Wind Atlas Methodology* was developed and described in the "European Wind Atlas" (Troen and Petersen, 1989). This methodology - as implemented in WASP - is now widely considered as the industry standard for wind resource estimation.

In the following sections the modeling framework of Risø will be described (Section 3.1) and in Section 3.3 a method developed within this project to infer the wind speed from a wind farm will be described and an example of its application given.

3.1. Risøs model framework for wind simulation and prediction

The Risø model suite for wind-power meteorology predicts wind climates, forecasts energy production, describes and simulates turbulence, and estimates extreme winds (Petersen et al., 1999a) (Petersen et al., 1999b). A brief introduction follows:

- The WASP model (Mortensen et al., 2002) is based on methods described in the European Wind Atlas (Troen and Petersen, 1989) and has become a worldwide standard for estimates of the wind energy potential at potential wind energy sites, see http://www.wasp.dk/. The model concept is to apply representative wind-climate data, typically sampled by national meteorological institutes, for estimates at new locations. The sampled data are analysed and corrected for local effects of terrain topography, surface roughness, nearby obstacles, and stability effects. Similar corrections, representative for the potential site, are reintroduced in the prediction phase. Terrain-induced speed-up is modelled by the outer-layer/inner-layer concept (Jackson and Hunt, 1975), i.e. with potential flow and local boundary layers. Obstacle shelter is also modelled by a linear flow model and effects of variable surface roughness is modelled by internal boundary layers. The effect of the overall roughness is modelled by the geostrophic drag law, which links the friction velocity to a geostrophic wind by a Rossby number

$$U_{\text{geo}} = \frac{u_*}{\kappa}\sqrt{\left(\ln\left(\text{Ro}\right) - A\right)^2 + B^2}, \quad \text{Ro} \equiv u_*/|f|\, z_0 \tag{31}$$

  The A and B constants in Equation 31 are stability dependent, and therefore the statistical relation between geostrophic- and surface winds is estimated by a combination of perturbation calculation and spatial interpolation between inland and offshore conditions. For convenience the wind climates are stored as tables of Weibull distributions.

  The energy production of a wind turbine is estimated by a power curve, predicting energy production for a standard air density as a function of the 10-min average wind speed

at turbine hub height. Characteristic features of the power curve are the cut-in speed where production starts ($\simeq$4 m/s), the regulation speed where rated power is reached ($\simeq$15 m/s), and the cut-out speed ($\simeq$25 m/s) where the turbines is stopped for safety reasons. The optimal design is a quick rise to rated power followed by a flat curve until cut-out speed. The annual energy production for a single turbine is predicted by convolution of the local wind-speed probability distribution and the power curve of the chosen turbine. The production by a wind farm involves an additional wake model based on a momentum balance specified by the rotor diameter and thrust-coefficient, which, like the power curve, is a function of wind speed, turbine aerodynamics, and regulation strategy. The over-all effect of wakes is that the first row of turbines steals part of the wind from the downwind turbines when the wind speeds is below regulation velocity. These wake calculations, called the PARK model, are now integrated in WASP and used to find the optimal layout of the wind farm.

- KAMM (Frank et al., 2001), developed by Karlsruhe University, is a meso-scale model which will predict certain phenomena out of reach of the linear flow models of WASP, e.g. valley winds and sea breezes. To take these effects into account, the KAMM/WASP method (Landberg and Watson, 1994) has been developed. The KAMM calculations are repeated for a range of geostrophic wind conditions and results are compiled for local wind climate statistics applicable as WASP input, see http://www.mesoscale.dk/. There are various methods for estimates of geostrophic wind statistics. Wind statistics might be extracted from radiosonde data or the NCEP/NCAR reanalysis data set covering the entire globe, see http://www.cdc.noaa.gov/. Another option is to generate statistics of geostrophic wind calculated by archived surface pressures.

- The coastal discontinuity model (CDM) is another model (Halliday et al., 2001), which has been used in combination with NCEP/NCAR reanalysis data. The influence of upwind land surfaces on the offshore wind speed profiles was modelled by a combined stability and internal boundary layer model based on principles similar to those of WASP. The advantage is that corrections were applied in each time step with varying sea fetch and stability conditions leading to better statistics of the offshore wind climate.

- Measure-correlate-predict (MCP) models are sometimes used as a supplement to WASP, in case a developer has installed an on-site meteorological station (Nielsen et al., 2001). Such data may be of good quality, but usually the measurement period is limited to one or two years, which is a poor basis for estimates of the long-term climate. The MCP method is to establish a statistical correlation, e.g. sector-wise linear regression, between the new measurements and data from a well-established near-by meteorological station. This statistical model is used to construct long-term statistics for the new site by long-term data from the reference station. Finally, the long-term statistics for the new site are used as input to WASP for prediction of annual power production by the selected turbines and park layout.

- PREDIKTOR (Landberg, 1999) is a tool for short-term wind energy production forecasts useful for the planning by power utilities, see http://www.prediktor.dk/. The system is implemented as an on-line facility with automatic updates published via the Internet. A weather-forecast model like DMI-HIRLAM supplies regional wind forecasts for a selected level, which is interpreted as the geostrophic wind and translated to surface winds

and energy production by the WASP/PARK method. The model includes local effects of terrain, surface roughness, obstacles, turbine power curves, and park layout. In order to further optimize the energy forecasts, the physical model is supplemented by empirical corrections based on model output statistics.

- WASP Engineering (Mann et al., 2002) is a tool for prediction and simulation of site-dependent turbulence, extreme wind and profiles, see www.waspengineering.dk/. The potential users are engineers designing optimal turbines with sufficient safety margins for fatigue damage and extreme loads. The mechanical loads on the constructions are typically estimated by computer simulation of structural vibrations of an operating turbine exposed to realistic turbulent fields simulated by WASP Engineering. The turbulence model is based on rapid-distortion theory (RDT), which predicts the spectral statistics of turbulent eddies being stretched or squeezed by the mean flow. Initial turbulence is modelled as an isotropic von Karman type spectral tensor, scaled by the energy dissipation rate and a single length scale. The isotropic turbulence is transformed to realistic turbulence by RDT corrections for boundary-layer shear, changes in surface roughness, and speed-up by terrain topography. For this purpose, the mean flow is modelled by LINCOM, which is a linear flow model similar to that of WASP except that it operates on a cartesian grid rather than a polar one. From the 3-D spectral tensor it is possible to extract information on power spectra of velocity components in any direction, cross spectra, and the spectral coherence of fluctuations at spatially separated points. The spectral tensor is also the basis for Fourier simulation of 3-D turbulence fields of three correlated velocity components. Using the 'frozen-turbulence' approximation, these 3-D spatial fields are interpreted as a sequences of 2-D fields hitting the wind turbine rotor. WASP Engineering will also translate regional geostrophic extreme-wind statistics to local wind-extreme statistics using the WASP corrections described above.

WASP is the most prominent member of the model family and, although primarily intended for turbine siting, it has been possible to extract or interchange modules and extend the use to other applications. In the present project the task is to assess whether wind turbine power production may predict surface winds – more or less a reverse PREDIKTOR problem. For this purpose we are mainly interested in the PARK module of WASP.

3.2. Predicting wind speed by measured power production

The relation between wind speed and energy production is provided by the wind-turbine power curve. This implies that useful information will only be available in the range between cut-in speed and the speed where the turbine reaches rated power ($\simeq$4–15 m/s). Outside this range the relation may be ambiguous, e.g. zero power output could both indicate wind speed below the cut-in speed or beyond cut-out. In practise, this is not a problem, since there should be some prior estimate of the likelihood of storm or calm. Suppose that we express this preliminary expectation as a probability distribution $f_s(s)$. Furthermore we have an expectation of the power production given a certain wind speed $f_{P|s}\ (P)$. Then we assess the conditional wind speed distribution $f_{s|P}\ (s)$ by Baye's rule using the probability distribution of expected power production

depending on wind speeds.

$$f_{s|P}\,(s) = \frac{f_s\,(s)\,f_{P|s}\,(P)}{\int\limits_0^\infty f_s\,(s)\,f_{P|s}\,(P)\,ds} \tag{32}$$

In the following section it is shown that wakes in wind-turbine parks introduce variability depending on wind direction, so we extend the formula to:

$$f_{s|P,\theta}\,(s) = \frac{f_s\,(s)\int\limits_0^{2\pi} f_{P|s,\theta}\,(P)\,d\theta}{\int\limits_0^{2\pi}\int\limits_0^\infty f_s\,(s)\,f_{P|s,\theta}\,(P)\,ds\,d\theta} \tag{33}$$

In search for the a priori probability distribution of wind speed and direction we first consider orthogonal components of the wind vector. One way to estimate the uncertainty of this is provided by the 'poor mans ensemble forecast', which is a weighted average of estimates by a sequence of recent forecasts.

$$\bar{u} = \sum w_j u_j \left(\sum w_j\right)^{-1} \quad \text{and} \quad \bar{v} = \sum w_j v_j \left(\sum w_j\right)^{-1} \tag{34}$$

Here, u_j and v_j are orthogonal wind components for forecast no. j and are corresponding weighted averages $(\bar{u}, \bar{v})$ based on weight coefficients, e.g. parameterized by an exponential decay $w_j = \exp\left(-j\Delta\tau/T\right)$, where $\Delta\tau$ is the time lag between each forecast). The variances of the weighted sums are

$$\begin{aligned}
\sigma_u^2 &= \left[\sum w_j u_j^2 + \bar{u}^2 \sum w_j - 2\bar{u}\sum w_j u_j\right]\left(\sum w_j\right)^{-1} \\
\sigma_v^2 &= \left[\sum w_j v_j^2 + \bar{v}^2 \sum w_j - 2\bar{v}\sum w_j v_j\right]\left(\sum w_j\right)^{-1} \\
\mathrm{Co}_{uv} &= \left[\sum w_j u_j v_j + \bar{u}\,\bar{v}\sum w_j - \bar{u}\sum w_j v_j - \bar{v}\sum w_j u_j\right]\left(\sum w_j\right)^{-1}
\end{aligned} \tag{35}$$

In polar coordinates, e.g. speed and direction, the vector is

$$s = \sqrt{u^2 + v^2} \quad \text{and} \quad \theta = \mathrm{Arctan2}\,(u, v) \tag{36}$$

and variances are estimated by

$$\begin{aligned}
\sigma_s^2 &= \left(\bar{u}^2 + \bar{v}^2\right)^{-2}\left(\bar{u}^2\sigma_v^2 + \bar{v}^2\sigma_u^2 + 2\bar{u}\,\bar{v}\,\mathrm{Co}_{uv}\right) \\
\sigma_\theta^2 &\simeq \left[\mathrm{Arcsin}\,(\varepsilon)\left(1 + \left(2\Big/\sqrt{3} - 1\right)\varepsilon^3\right)\right]^2
\end{aligned} \tag{37}$$

using

$$\varepsilon^2 = \left(\bar{u}^2 + \bar{v}^2\right)^{-4}\left[\bar{u}^2\sigma_v^2 + \bar{v}^2\sigma_u^2 - 2\bar{u}\,\bar{v}\,\mathrm{Co}_{uv}\right] \tag{38}$$

Here, the directional variance is estimated by a formula which approaches the traditional 'small-angle' estimate $\sigma_\theta \simeq \varepsilon$ for $\varepsilon \to 0$ (Yamartino, 1984).

The ensemble approach is only used for estimates of uncertainty, whereas the most recent forecast is used for the expectation value. Expectation values and uncertainties deduced from

Table 4: Positions of the individual turbines in the Abild wind farm.

	UTM N (km)	UTM E (km)
Turbine no. 1	6093.530	492.960
Turbine no. 2	6093.659	492.944
Turbine no. 3	6093.788	492.927
Turbine no. 4	6093.591	493.069
Turbine no. 5	6093.720	493.053
Sonofon mast	6093.136	492.532

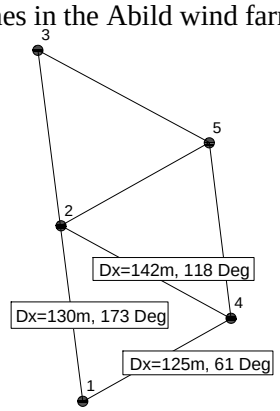

HIRLAM forecasts are used to scale a priori distributions for wind speed $f_s(s)$ and direction $f_\theta(\theta)$. The normal distribution is applied for both variables, since the wind-speed standard deviation is assumed small compared to the average speed, and directional standard deviation is assumed small compared to 2π. The expected power production, depending on speed and direction, is known by WASP analysis, and a realistic variability is estimated by the error analysis used in power-curve calibration tests (Pedersen, 1993). With the expected mean production and variance we model the conditional probability distribution $f_{P|s,\theta}(P)$, again by a normal distribution. Finally, the a posteori wind-speed distribution is calculated by equation 33.

3.3. A study of wind and energy production at Abild wind turbine park

As a test case we have studied data from the Abild wind farm located in flat terrain ≈4km N of Tønder and ≈10km from the sea. Measurements and background information were communicated by ELTRA, whilst DMI extracted a corresponding series of wind speeds at hub height from historical HIRLAM forecasts. The farm is designed as rows of turbines oriented along the 173° direction with three turbines in the predominating upwind row and two turbines in the rear row, see Table 4. Distances between turbines is 130m within the main rows and 125m or 142m between turbines in separate rows for the directions 61° or 118°, respectively. The turbine model is Wind World 3700, which has a rated power of 550kW. The power curve was known in advance and NEG-Micon (new owner of Wind World) supplied an approximate calculated thrust-coefficient curve. From previous projects, digital maps of terrain and surface-roughness were available in the standard WASP format. These digital maps were originally derived from information by Kort & Matrikelstyrelsen, and our partners at Energi- & Miljø Data processed the surface-roughness data. The regional wind climate was available from the same project, where it was calculated by measurements from the DMI station at Vester Vedsted during 1987-96. Local obstacles were neglected; the closest buildings are ≈100m toward WNW measured from the closest turbine, whereas Abild village is ≈1000m toward SW.

Additional signals are available from sensors mounted on a telecommunication mast (Sonofon) approximately $1/2$km S of the farm. This station is equipped with two anemometers, a wind vane and a temperature sensor. The ratio of the anemometer signal difference over their mean is shown in Figure 32. There are signs of flow distortion and for this analysis we select data

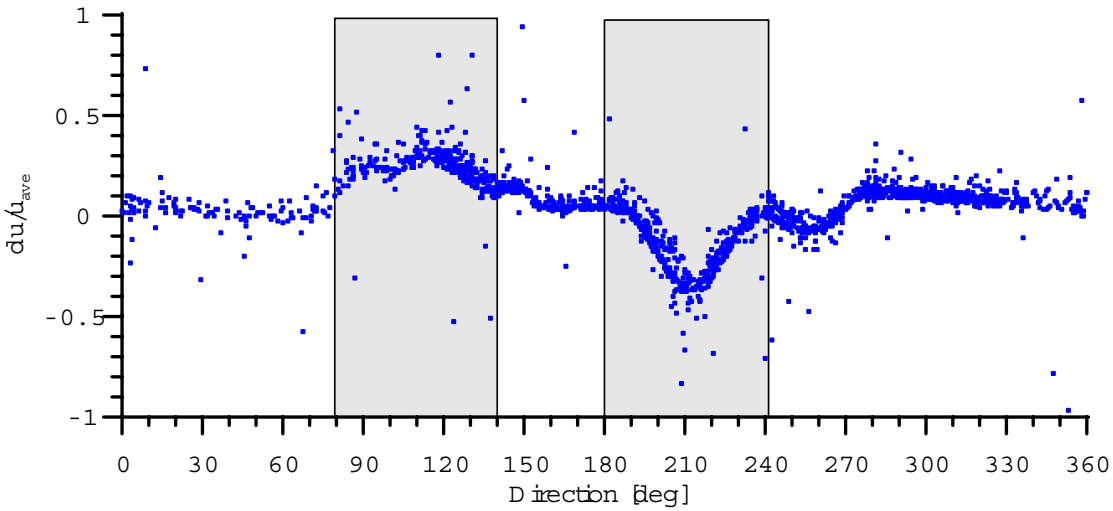

Figure 32: The ratio $2(u_1 - u_2)/(u_1 + u_2)$ as a function of wind direction.

from the first anemometer with wind directions in the sector 80-140° data from the second anemometer with directions in the sector 180-240° and the average speed otherwise, provided that both signals are available. The database was screened for obvious outliers. Wind speeds measured prior to October 4, 2001 were corrected with a factor of 1.33 (ELTRA, personal communication) and, in addition a height correction from measurement height (35m) to hub height (42m) was applied, assuming logarithmic profiles and a surface roughness of z_0=0.03m. The farm was analysed by WASP 7.2 and the over-all production loss was found to be modest 9%, see Figure 33. The wake-effect may, however, be much larger for specific combinations of speed and direction, in particular for weak winds and when turbines are aligned in the wind direction, see Figure 34. This figure is calculated by WASP using 1° directional resolution. The most sensitive directions are 118°/298° (three turbines sheltered) and 173°/353° or 61°/241° (two turbines sheltered). Weaker wake effects are observed for the directions 26°/206° (turbines no. 1 and 5 aligned) or 144°/324° (turbines no. 3 and 4 aligned). No production loss is expected for wind speeds beyond 15 m/s when power regulation starts. The figure illustrates the importance of knowing the wind direction when predicting speeds by power production with wake effects.

Figure 35 shows the empirical relation between wind speed and production. The shape is in general agreement with WASP predictions shown by a solid curve. Situations with expected minimal and maximal wake effect are indicated by blue and red dots and, although a slight distinction is observed, this does not explain all of the variance. The plot is repeated for 10-min averaging time, compatible with HIRLAM predictions, and for 1-hour averaging time. The longer averaging-time reduces the scatter, probably because this time-resolution is in better accordance with the WASP model and because of better spatial correlation of winds in the park and at the reference mast, $\approx 1/2$km apart. For higher wind speeds the marked points falls on three tracks, suggesting that the park operated with only three or four turbines for part of the period. Unfortunately, statistics of turbine stops are unavailable. Mean and standard deviations the 1-hour data are shown in Figure 36. The model seems to underestimate the power production slightly, or as an alternative explanation, the reference wind speeds measured at the Sonofon mast could be too low.

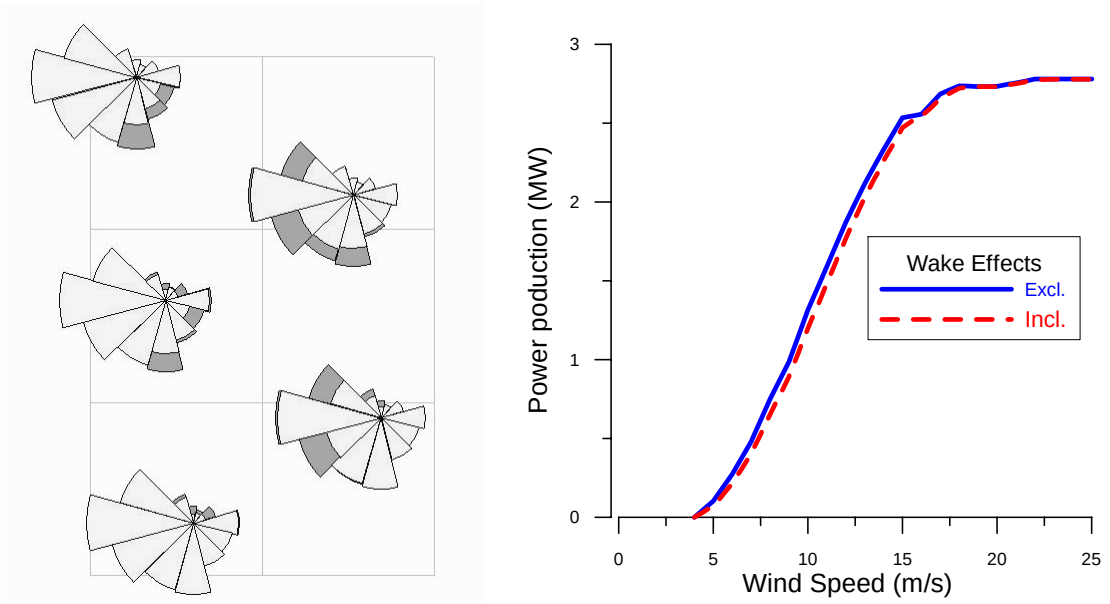

Figure 33: a) Predicted annual production of individual turbines as a function of wind direction and b) the park-scale power curve independent of wind direction.

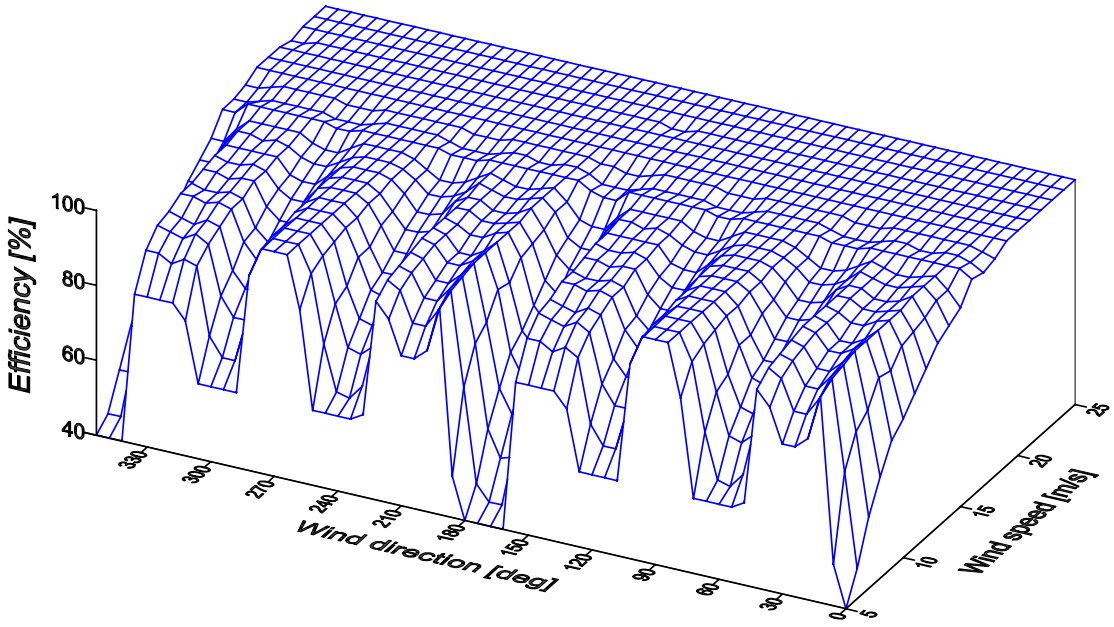

Figure 34: Relative loss of production by wake effects as a function of wind speed and direction.

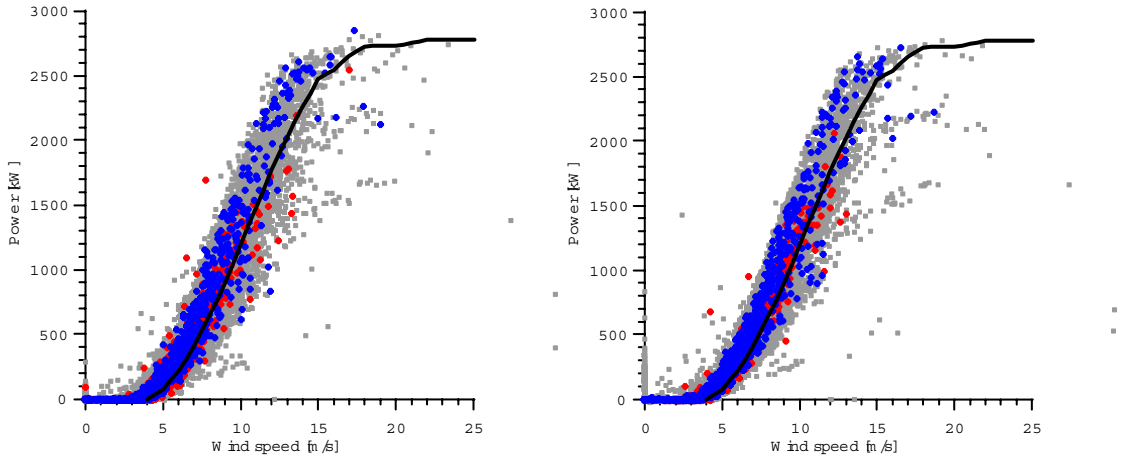

Figure 35: Coincident measurements of wind speed and power production during 2000–2001 with 10-min (left) or 1-hr (right) averaging time. Blue and red dots indicates measurements with wind directions 85–95°/265–275° and 168–178°/168–178°, respectively. The solid curve is the model prediction.

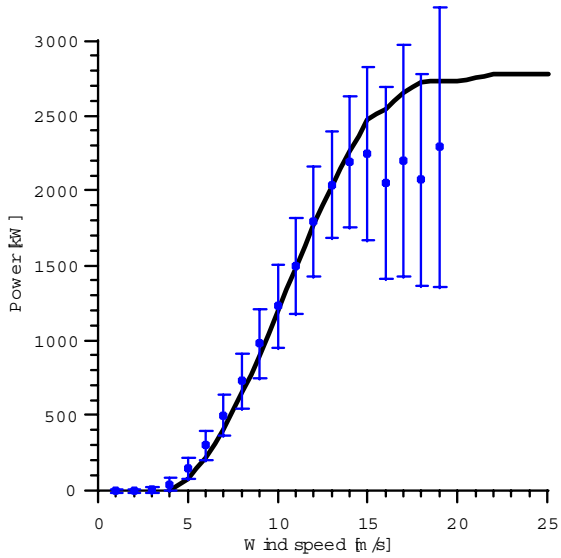

Figure 36: Mean and standard deviations of measured power productions as a function of wind speed.

The power measurements and HIRLAM forecasts are used for wind-speed prediction by equation 33 and compared with measurements at the Sonofon mast. The a priori prediction of wind speed and direction are assumed Gaussian with mean values equal to the most recent forecast and variances estimated by Equation 37 using a 12-hour exponential decay for the weight coefficients. The expected power production extracted from WASP is a function of wind speed and direction. The power-curve uncertainty is estimated in accordance with certification standards (Pedersen, 1993), although Figure 35 indicates that actual scatter was considerably higher. Figure 37 compares series of HIRLAM forecasts, the predictions, and local measurements and the predictions are seen to be closer to the local measurements than the raw forecasts. Also shown are the estimated uncertainty and observed differences between forecasts and local measurements. The HIRLAM uncertainty estimated by Equation 37 is in agreement with observed differences relative to local data, whereas estimated uncertainties of predictions seem far too optimistic. The most likely explanation is that power production is less predictable than expected. An alternative prediction was made with empirical power uncertainty as observed in Figure 36. This test provided realistic uncertainty estimates of the predictions, but unfortunately the bias of the alternative method was less ideal than with the first approach. Figure 38 shows monthly statistics of discrepancies between HIRLAM forecasts and local measurements or similar for the predictions. The monthly bias is always improved by the production-based estimates with no systematic seasonal dependence. The standard deviation is usually improved by a factor of two.

The conclusion is that it *is* possible to improve the forecast by knowledge of current wind power production. The method could be improved with access to more detailed information, e.g. the production of individual turbines or, even better, from isolated wind turbines not exposed to the wakes of upstream turbines. Signals from the nacelle anemometer are also of interest, especially when a correlation with the free-stream velocity has been established and when the turbine yaw signal is available (Antoniou et al., 1998). Data from anemometers sometimes mounted on near-by masts would provide ideal information.

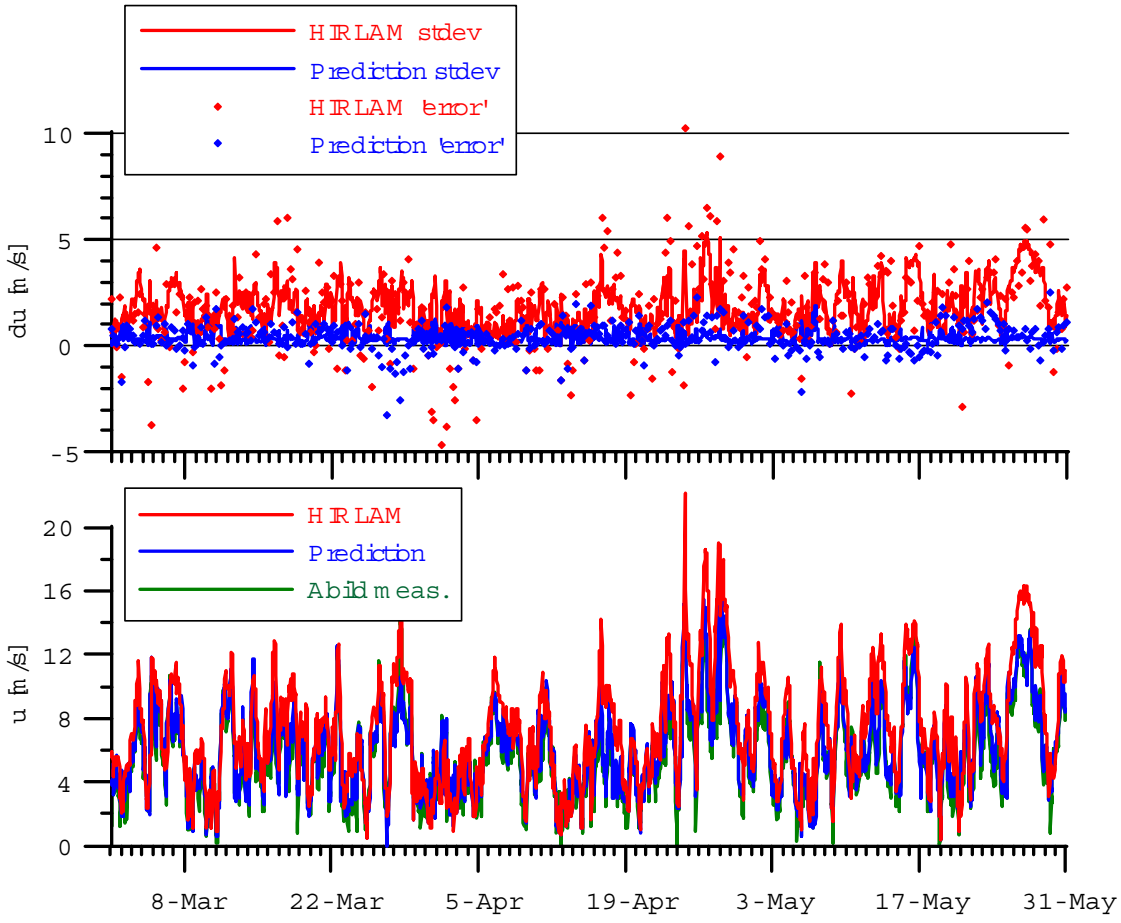

Figure 37: Comparison between HIRLAM forecasts, predictions using power signal, and local measurements. The top frame shows estimated uncertainty (lines) and observed differences relative to local measurements.

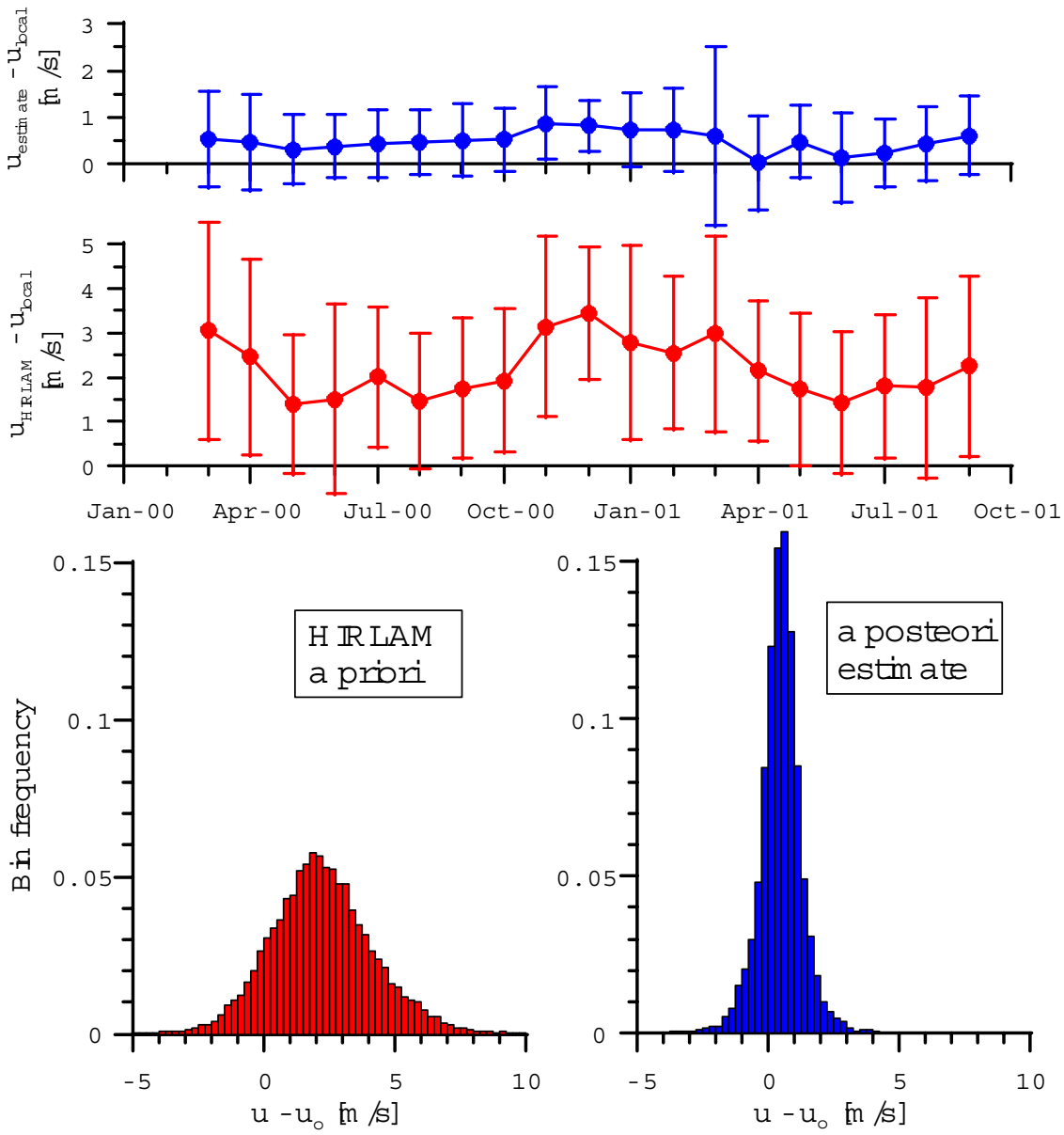

Figure 38: a) Monthly mean and RMS value of differences between forecast and local measurements (red) and a posteori estimates derived from power production (blue). b) Corresponding Histograms of data from all periods.

3.4. Other studies during the project

A five month integration (October 2000 to March 2001) has been carried out with 6 hourly ECMWF analysis increments on a 1.0° scale. This approach keeps the model close to the correct atmospheric state. Any improvements will therefore show up as relatively small differences. The statistical signal from 600 times 6 hour forecasts is very stable.

The model was run in three versions: One uncoupled version and two coupled versions. The difference between the two coupled versions was with respect to the parameter exchanged between DMI-WAM and DMI-HIRLAM. One experiment ('v10m') exchanges 10 metre wind while the other experiment ('stress') exchanges the surface stress. The model resolution in HIRLAM was 0.45° with 31 vertical levels. The model integration area was selected such that the typical storm track the Atlantic from the USA to the northern part of Norway was covered. The model grid does not cover the part of the Atlantic with a large percentage of ice, because the parameterization in WAM is not yet developed for this. The model grid contains a large fraction of the Atlantic Gulf Stream which is very critical for mid-latitude weather prediction. This area is associated with strong currents and a strong horizontal temperature gradient in the surface temperature. The wave structure is normally very complicated along the polar front, which implies that the sea surface is very rough. The nature of the polar front is that the position can change rather rapidly, but the width of the polar front is less than 100 km. Another issue is the static stability. Because of the sharpness of the polar front's sea surface temperature gradient, the atmospheric model's static stability may become incorrect near the front. Thus the full benefit of the coupling between an atmospheric model and a wave model may only be achieved when an ocean model is included as well.

The focus of this particular run is on an examination of the possible benefit of the ocean coupling on actual wind energy estimates on land stations. Most wind energy capacity in Europe is installed in a belt around 10 km from the sea. We focus on 4 Danish stations in Jutland in the vicinity of a coast. Two stations (Frederikshavn and Århus) have been chosen on the east coast while Rømø and Hvide Sande have been selected near the west coast. A module called every time step in DMI-HIRLAM has been developed which can deduce a wind power estimate for a given station. This is done by combining wind information with a standard power curve for the site(s). The results of such computations and comparisons with measured power production are given in tables 5a and 5b.

The results for the 5 month long period described above indicate that

- The effect of wave coupling on wind prediction over land is on average small, but for the the North Sea coastline the results for estimated wind power suggest an improvement of the coupling around 2.5 %.
- Improvements more than 100 km inland for onshore wind conditions indicate that the coupling has a positive large scale effect on the forecast.
- The stations on the North Sea coastline and 100 km away show almost the same error statistics.
- The results for stress coupling run are marginally better than the 10m wind coupled run.

Table 5a:
Statistics for energy production at the two sites (Frederikshavn and Århus) on the east coast. The average mean error (bias), mean absolute error (abs) and root mean square error (rms) are given for all wind directions, and for directions 0-179°, and 180 - 360°. Uncoupled results for wind and the two different coupled results are shown in separate columns. The improved prediction of energy production in percent is given in the last column.

EAST coast	-	-	-	-	-	-
- -	Direction deg.	Number of obs	Uncoupled	Coupled v10m	Coupled stress	Improvement %
bias:	0-359°	7196	2.51	2.45	2.44	2.9
abs:	0-359°	7196	2.60	2.54	2.53	2.5
rms:	0-359°	7196	4.38	4.29	4.29	2.1
bias:	0-179°	3211	2.32	2.24	2.24	3.7
abs:	0-179°	3211	2.44	2.36	2.36	3.2
rms:	0-179°	3211	4.03	3.92	3.91	3.0
bias:	180-359°	3981	2.67	2.61	2.61	2.3
abs:	180-359°	3981	2.74	2.68	2.68	2.1
rms:	180-359°	3981	4.64	4.57	4.57	1.6

Table 5b:
Statistics for energy production at the two sites (Rømø and Hvide Sande) on the west coast. The average mean error (bias), mean absolute error (abs) and root mean square error (rms) are given for all wind directions, and for directions 0-179°, and 180 - 360°. Uncoupled results for wind and the two different coupled results are shown in separate columns. The improved prediction of energy production in percent is given in the last column.

WEST coast	-	-	-	-	-	-
- -	Direction deg.	Number of obs	Uncoupled	Coupled v10m	Coupled stress	Improvement %
bias:	0-359°	4509	2.58	2.50	2.50	3.3
abs:	0-359°	4509	2.80	2.73	2.73	2.5
rms:	0-359°	4509	4.64	4.54	4.54	2.1
bias:	0-179°	2615	2.50	2.40	2.40	3.8
abs:	0-179°	2615	2.74	2.65	2.66	2.9
rms:	0-179°	2615	4.56	4.45	4.45	2.4
bias:	180-359°	1894	2.70	2.63	2.63	2.6
abs:	180-359°	1894	2.90	2.83	2.84	2.1
rms:	180-359°	1894	4.74	4.66	4.67	1.6

4. Conclusions

It is possible to draw a number of conclusions from the various studies carried out during the project.

The results described in section 2 show that the effect of coupling DMI-HIRLAM with an ocean wave model is positive, although quite modest in its present form. Wind biases appear to be reduced in the fully coupled runs. Also the results indicate that synoptic scale forecast improvements are best achieved if the coupling is implemented for a large model domain. Improved quality has been obtained when increasing the horizontal model resolution from 0.45° to 0.15° The impact of increased vertical resolution appears to be more marginal.

The coupling experiments mentioned in section 3.4 indicate that the effect of wave coupling on the quality of wind (and wind power) prediction may be larger over the ocean than over land. The results suggest a potential for improving the forecast of wind power production by 2.5 % at the Danish North Sea coastline.

The coupling method as currently implemented has some weaknesses which may be improved in the future. The stress computation as included in WAM assumes a neutral drag coefficient in the atmospheric surface layer. This is somewhat inconsistent with the stability dependent stress computation in DMI-HIRLAM, which is also connected to the 10m wind computation in DMI-HIRLAM. Since WAM is currently calibrated to the 10m wind data from the atmospheric model there is no guarantee that using stress from DMI-HIRLAM will produce better results prior to a recalibration of WAM. However, the results of using stress coupling appear to be marginally better than the alternative of using 10 metre wind, and an improved forcing of WAM in the future should involve stress from HIRLAM rather than 10m wind. A fully consistent coupling would involve a computationally more expensive iterative procedure for determination of surface fluxes.

An increase of the directional resolution of the WAM spectrum from 12 to 18 or 24 directions may lead to improved results of the coupling as found recently in the ECMWF model. At a later stage it may pay off to extend the coupling to a complete ocean model including ocean currents. This provides a better framework for describing sea surface temperatures in areas with large horizontal temperature gradients affecting often the development of new weather systems.

Also the character of the turbulence scheme used in DMI-HIRLAM has a fundamental impact on the wind profiles achieved in the the model. It has been shown that the modified vertical diffusion scheme mentioned in section 2.4.5 improves the representation of the vertical wind profile in the atmospheric boundary layer. This confirms that the turbulence parameterization is vital and should be considered in the context of future improvements of the forecasting system.

A new method for improvement of wind forecasts from DMI-HIRLAM by local power-production data is suggested. Comparison with independent local wind speed data proved it was possible to reduce bias and standard deviation of the local wind speed prediction. These reductions were however smaller than anticipated, suggesting that the power production was influenced by occasional wind turbine stops or that reference wind speed measurements had some flow distortion. The method should work better with data from individual wind turbines, since this would avoid the problems of stopped turbines or false wake-corrections due to uncertain local wind directions.

5. Acknowledgements

The present work has been financed by the Danish Ministry of Energy (Energistyrelsen), contract 1363/00-0020. The work of Jess U Jørgensen, Corinna Moerlen and Jacob Woge Nielsen is greatly appreciated.

The measurements from ‘Horns Rev’ and south of ‘Læsø’ have been established as a part of ‘Havvindmøllepålægget’.

References

Antoniou, I., Pedersen, T., and Markkilde Petersen, S. (1998). Comparing the power performance results by using the nacelle and the mast anemometer. In Watson, R., editor, *European wind energy conference. Proceedings. EWEC '97, Dublin (IE), 6-9 Oct 1997*, pages 229–233. Irish Wind Energy Association, Slane.

Bidlot, J., Janssen, P., B.Hansen, and Günther, H. (1997). A modified set up of the advection scheme in the ECMWF wave model. Technical Report 237, European Center for Medium Range Weather Forecasts.

Brutsaert, W. (1975). The roughness length for water vapor, sensible heat and other scalars. *J. Atmos. Sci.*, 32:2028–2031.

Businger, J. A., Wyngaard, J. C., Izumi, Y., and Bradley, E. F. (1971). Flux-profile relationships in the atmospheric surface layer. *J. Atmos. Sci.*, 28:181–189.

Chalikov, D. and Makin, V. (1991). Models of the wave boundary layer. *Bound. Layer Meteorol.*, 56:83–99.

Charnock, H. (1955). Wind stress on a water surface. *Quart. J. Roy. Meteorol. Soc.*, 81:639–640.

Clayson, C. A., Fairall, C. W., and Curry, J. A. (1996). Evaluation of turbulent fluxes at the ocean surface using surface renewal theory. *J. Geophys. Res.*, 101(C12):28503–28513.

Cuxart, J., Bougeault, P., and Redelsperger, J.-L. (1995). Turbulence closure for a non-hydrostatic model. In *12th AMS symp. on Boundary Layer Turbulence*, pages 409–412.

Cuxart, J., Bougeault, P., and Redelsperger, J.-L. (2000). A turbulence scheme allowing for meso-scale and large-eddy simulations. *Quart. J. Roy. Meteorol. Soc.*, 126:1–30.

Deardorff, J. W. (1972). Theoretical expression for the countergradient vertical heat flux. *J. Geophys. Res.*, 77:5900–5904.

DeCosmo, J., Katsaros, K. B., Smith, S. D., Anderson, R. J., Oost, W. A., Bumke, K., and Chadwick, H. (1996). Air-sea exchange of water vapour and sensible heat: The Humidity Exchange Over the Sea (HEXOS) results. *J. Geophys. Res.*, 101(C5):12001–12016.

Donelan, M. (1982). The dependence of the aerodynamic drag coefficieent on wave parameters. Proc. first int. conf. on meteorology and air-sea interaction of the coastal zone, The Hague, Amer. Meteorol. Soc.

Frank, H. P., Rathmann, O., Mortensen, N. G., and Landberg, L. (2001). The numerical wind atlas - the KAMM/WA^{S}P method. Technical Report Risø-R-1252(EN), Risø National Laboratory.

Garrat, J. R. (1992). *The Atmospheric Boundary Layer*. Cambridge University Press.

Günther, H., Hasselmann, S., and Janssen, P. (1992). Wamodel cycle4 (revised version). Technical Report 4, Deutches Klimarechnenzentrum.

Halliday, J., Watson, G., Palutikof, J., Holt, T., Barthelmie, R., Coelingh, J., Folkerts, L., Zuylen, E. v., and Cleijne, J. (2001). Power - a methodology for predicting offshore wind energy resources. In Helm, P. and Zervos, A., editors, *2001 European wind energy conference and exhibition, Copenhagen (DK), 2-6 Jul 2001*, pages 785–788.

Hansen, C. and Larsen, S. E. (1997). Further work on the Kitaigorodskii roughness length model: A new derivation using Lettau's expression on steep waves. *Geophysica*, 33(2):29–44.

Hansen, H., Johnson, H., Hojstrup, J., and Lange, B. (1998). Wind-wave modeling in waters with restricted fetches. Technical Report 27-30 January, 5th International Workshop on Wave Hindcasting and Forecasting.

Hansen, J. C. and Tande, J. O. G. (1993). Are feasibility studies reliable at high energy penetration levels. In Garrad, A., Palz, W., and Scheller, S., editors, *European wind energy conference and exhibition, Lübeck–Travemünde (DE), 8-12 Mar. 1993*, pages 359–362. (H.S. Stephens and Associates, Bedford (UK)).

Hersbach and Janssen, P. (1999). Improvement of the short-fetch behavior in the wave ocean model (WAM). *J. Atmos. & Ocean Tech.*, 16:884–892.

Jackson, P. and Hunt, J. (1975). Turbulent wind flow over a low hill. *Quart. J. Roy. Meteorol. Soc.*, 101:929–955.

Janssen, P., J.D.Doyle, Bidlot, J., Hansen, B., Isaksen, L., and Viterbo, P. (2001). Impact and feedback of ocean waves on the atmosphere. Technical memorandum no. 341, ECMWF.

J.She and Nielsen, J. (1999). Operational wave forecasts in Baltic and North Sea. *Danish Meteorological Institute*, DMI Sci. Rep. 99-07.

K. Hasselmann, K., Barnett, T., Bouws, E., Carlson, H., Cartwright, D., K.Enke, Ewing, J., Gienapp, H., Hasselmann, D., Kruseman, P., Meerburg, A., Muller, P., Olbers, D., Richter, K., Sell, W., and Walden, H. (1973). Measurements of wind-wave growth and swell decay during the Joint North Sea Wave Project (JONSWAP). Technical report, A8Deut. Hydrogr. Z., A8(12).

Källén, E. (1996). HIRLAM Documentation Manual. system 2.5. *SMHI, Norrköping, Sweden*.

Komen, G., Cavaleri, L., Donelan, M., Hasselmann, K., Hasselmann, S., and Janssen:, P. (1994). *Dynamics and modelling of ocean waves*. Cambridge University Press.

Landberg, L. (1999). Short-term prediction of the power production from wind farms. *J. Wind Eng. Ind. Aerodyn.*, 80:207–220.

Landberg, L. and Watson, R. (1994). The new irish wind resource atlas. In *In Proceedings from EWEA 94, Thessaloniki, Vol. 1*, pages 233–237.

Lenderink, G. (2002). Recent and future developments in turbulence modelling in hirlam. *HIRLAM Newsletter*, 41:55–60.

Liu, W. T., Katsaros, K. B., and Businger, J. A. (1979). Bulk parameterization of air-sea interaction of heat and water vapor including the molecular constraints at the interface. *J. Atmos. Sci.*, 36:1722–1735.

Louis, J.-F. (1979). A parametric model of vertical eddy fluxes in the atmosphere. *Boundary-Layer Meteorol.*, 17:187–202.

Louis, J. F., Tiedtke, M., and Geleyn, J. F. (1982). A short history of the operational PBL parameterization at ECMWF. In *Workshop on Boundary Layer Parameterization*, pages 59–79, ECMWF, Reading.

Lundtang, E., Troen, I., Frandsen, S., and Hedegaard, K. (1981). Danish wind atlas. Risø -r-428, Risø National Laboratory.

Maat, N., Kraan, C., and Oost, W. A. (1991). The roughness of wind waves. *Boundary-Layer Meteorol.*, 54:89–103.

Machenhauer, B. (1988). HIRLAM final report. *HIRLAM Tech. Report*, 5:1–116.

Mann, J., Ott, S., Jørgensen, B. H., and Frank, H. (2002). iii WA^{s}P Engineering 2000. Technical Report Risø–R–1356(EN), Risø National Laboratory.

Mortensen, N., Heathfield, D., Landberg, L., Rathmann, O., Troen, I., and Petersen, E. (2002). Wind atlas analysis and application program. WAsP 7 Help Facility. ISBN 87-550-2941-8.

Nielsen, J. W., Jørgensen, J. B., and She, J. (2002). Verification of wave forecasts: DMI-WAM nov-dec 2001. Technical Report 02-18, Danish Meteorological Institute.

Nielsen, M., Landberg, L., Mortensen, N. G., Barthelmie, R., and Joensen, A. (2001). Measure-correlate-predict for wind resource assessment. In Helm, P. and Zervos, A., editors, *2001 European wind energy conference and exhibition, Copenhagen (DK), 2-6 Jul 2001*, pages 773–776.

Oost, W. A. (1998). The KNMI HEXMAX stress Data Reanalysis. *Boundary-Layer Meteorol.*, 86:447–468.

Pedersen, T. F. (1993). Recommendation for wind turbine power curve measurements. Technical Report Risø-I-745(EN), Risø National Laboratory.

Petersen, E. L., Mortensen, N. G., Landberg, L., Højstrup, J., and Frank, H. P. (1999a). Wind power meteorology. part I: Climate and turbulence. *WIND*, 1:25–45.

Petersen, E. L., Mortensen, N. G., Landberg, L., Højstrup, J., and Frank, H. P. (1999b). Wind power meteorology. part II: Siting and models. *WIND*, 1:55–72.

Petersen, E. L., Troen, I., Frandsen, S., and Hedegaard, K. (1981). Danish Windatlas. A rational method of wind energy siting. Technical Report Risø-R-428, Risø National Laboratory.

Sass, B. H., Nielsen, N. W., Jørgensen, J. U., Amstrup, B., and Kmit, M. (2002). The operational DMI-HIRLAM system. DMI tech. rep. no. 02-06, Danish Meteorological Institute.

She, J. (2000). Hirlam-wam quality assessment on winds and waves in the North Sea. Technical Report Scientific Report 00-27, Danish Meteorological Institute.

Smith, S., Anderson, R., Oost, W., Kraan, C., Maat, N., de Cosmo, J., Katsaros, K., Davidson, K., Bumke, K., Hasse, L., and Chadwick, H. (1992). Sea surface wind stress and drag coefficients: The hexos results. *Bound. Layer Meteorol.*, 60:109–142.

Troen, I. and Petersen, E. L. (1989). *European Wind Atlas*. Risø National Laboratory, Roskilde, DK.

Undén, P., Rontu, L., Calvo, J., Cats, G., Cuxart, J., Eerola, K., Fortelius, C., Garcia-Moya, J. A., Gustafsson, N., Jones, C., Järvenoja, S., Järvinen, H., Lynch, P., McDonald, A., McGrath, R., Nvascues, B., Ødegaard, V., Rodriguez, E., Rummukainen, M., Rõõm, R., Sattler, K., Savijärvi, H., Sass, B. H., Schreur, B. W., The, H., and Tijm, S. (2002). The HIRLAM-5 scientific documentation. HIRLAM-5 project, SMHI Norrköping, Sweden.

Yamartino, R. J. (1984). A comparison of several ”single-pass” estimators of the standard deviation of wind direction. *J. Climate Appl. Meteor.*, 23:1362–1366.

DANISH METEOROLOGICAL INSTITUTE

Scientific Reports

Scientific reports from the Danish Meteorological Institute cover a variety of geophysical fields, i.e. meteorology (including climatology), oceanography, subjects on air and sea pollution, geomagnetism, solar-terrestrial physics, and physics of the middle and upper atmosphere.

Reports in the series within the last five years:

No. 97-1
E. Friis Christensen og C. Skøtt: Contributions from the International Science Team. The Ørsted Mission - a pre-launch compendium

No. 97-2
Alix Rasmussen, Sissi Kiilsholm, Jens Havskov Sørensen, Ib Steen Mikkelsen: Analysis of tropospheric ozone measurements in Greenland: Contract No. EV5V-CT93-0318 (DG 12 DTEE):
DMI's contribution to CEC Final Report Arctic Trophospheric Ozone Chemistry ARCTOC

No. 97-3
Peter Thejll: A search for effects of external events on terrestrial atmospheric pressure: cosmic rays

No. 97-4
Peter Thejll: A search for effects of external events on terrestrial atmospheric pressure: sector boundary crossings

No. 97-5
Knud Lassen: Twentieth century retreat of sea-ice in the Greenland Sea

No. 98-1
Niels Woetman Nielsen, Bjarne Amstrup, Jess U. Jørgensen: HIRLAM 2.5 parallel tests at DMI: sensitivity to type of schemes for turbulence, moist processes and advection

No. 98-2
Per Høeg, Georg Bergeton Larsen, Hans-Henrik Benzon, Stig Syndergaard, Mette Dahl Mortensen: The GPSOS project
Algorithm functional design and analysis of ionosphere, stratosphere and troposphere observations

No. 98-3
Mette Dahl Mortensen, Per Høeg: Satellite atmosphere profiling retrieval in a nonlinear troposphere
Previously entitled: Limitations induced by Multipath

No. 98-4
Mette Dahl Mortensen, Per Høeg: Resolution properties in atmospheric profiling with GPS

No. 98-5
R.S. Gill and M. K. Rosengren: Evaluation of the Radarsat imagery for the operational mapping of sea ice around Greenland in 1997

No. 98-6
R.S. Gill, H.H. Valeur, P. Nielsen and K.Q. Hansen: Using ERS SAR images in the operational mapping of sea ice in the Greenland waters: final report for ESA-ESRIN's: pilot projekt no. PP2.PP2.DK2 and 2nd announcement of opportunity for the exploitation of ERS data projekt No. AO2..DK 102

No. 98-7
Per Høeg et al.: GPS Atmosphere profiling methods and error assessments

No. 98-8
H. Svensmark, N. Woetmann Nielsen and A.M. Sempreviva: Large scale soft and hard turbulent states of the atmosphere

No. 98-9
Philippe Lopez, Eigil Kaas and Annette Guldberg: The full particle-in-cell advection scheme in spherical geometry

No. 98-10
H. Svensmark: Influence of cosmic rays on earth's climate

No. 98-11
Peter Thejll and Henrik Svensmark: Notes on the method of normalized multivariate regression

No. 98-12
K. Lassen: Extent of sea ice in the Greenland Sea 1877-1997: an extension of DMI Scientific Report 97-5

No. 98-13
Niels Larsen, Alberto Adriani and Guido DiDonfrancesco: Microphysical analysis of polar stratospheric clouds observed by lidar at McMurdo, Antarctica

No.98-14
Mette Dahl Mortensen: The back-propagation method for inversion of radio occultation data

No. 98-15
Xiang-Yu Huang: Variational analysis using spatial filters

No. 99-1
Henrik Feddersen: Project on prediction of climate variations on seasonel to interannual timescales (PROVOST) EU contract ENVA4-CT95-0109: DMI contribution to the final report: Statistical analysis and post-processing of uncoupled PROVOST simulations

No. 99-2
Wilhelm May: A time-slice experiment with the ECHAM4 A-GCM at high resolution: the experimental design and the assessment of climate change as compared to a greenhouse gas experiment with ECHAM4/OPYC at low resolution

No. 99-3
Niels Larsen et al.: European stratospheric monitoring stations in the Artic II: CEC Environment and Climate Programme Contract ENV4-CT95-0136. DMI Contributions to the project

No. 99-4
Alexander Baklanov: Parameterisation of the deposition processes and radioactive decay: a review and some preliminary results with the DERMA model

No. 99-5
Mette Dahl Mortensen: Non-linear high resolution inversion of radio occultation data

No. 99-6
Stig Syndergaard: Retrieval analysis and methodologies in atmospheric limb sounding using the GNSS radio occultation technique

No. 99-7
Jun She, Jacob Woge Nielsen: Operational wave forecasts over the Baltic and North Sea

No. 99-8
Henrik Feddersen: Monthly temperature forecasts for Denmark - statistical or dynamical?

No. 99-9
P. Thejll, K. Lassen: Solar forcing of the Northern hemisphere air temperature: new data

No. 99-10
Torben Stockflet Jørgensen, Aksel Walløe Hansen: Comment on "Variation of cosmic ray flux and global coverage - a missing link in solar-climate relationships" by Henrik Svensmark and Eigil Friis-Christensen

No. 99-11
Mette Dahl Meincke: Inversion methods for atmospheric profiling with GPS occultations

No. 99-12
Hans-Henrik Benzon; Laust Olsen; Per Høeg: Simulations of current density measurements with a Faraday Current Meter and a magnetometer

No. 00-01
Per Høeg; G. Leppelmeier: ACE - Atmosphere Climate Experiment

No. 00-02
Per Høeg: FACE-IT: Field-Aligned Current Experiment in the Ionosphere and Thermosphere

No. 00-03
Allan Gross: Surface ozone and tropospheric chemistry with applications to regional air quality modeling. PhD thesis

No. 00-04
Henrik Vedel: Conversion of WGS84 geometric heights to NWP model HIRLAM geopotential heights

No. 00-05
Jérôme Chenevez: Advection experiments with DMI-Hirlam-Tracer

No. 00-06
Niels Larsen: Polar stratospheric clouds microphysical and optical models

No. 00-07
Alix Rasmussen: "Uncertainty of meteorological parameters from DMI-HIRLAM"

No. 00-08
A.L. Morozova: Solar activity and Earth's weather. Effect of the forced atmospheric transparency changes on the troposphere temperature profile studied with atmospheric models

No. 00-09
Niels Larsen, Bjørn M. Knudsen, Michael Gauss, Giovanni Pitari: Effects from high-speed civil traffic aircraft emissions on polar stratospheric clouds

No. 00-10
Søren Andersen: Evaluation of SSM/I sea ice algorithms for use in the SAF on ocean and sea ice, July 2000

No. 00-11
Claus Petersen, Niels Woetmann Nielsen: Diagnosis of visibility in DMI-HIRLAM

No. 00-12
Erik Buch: A monograph on the physical oceanography of the Greenland waters

No. 00-13
M. Steffensen: Stability indices as indicators of lightning and thunder

No. 00-14
Bjarne Amstrup, Kristian S. Mogensen, Xiang-Yu Huang: Use of GPS observations in an optimum interpolation based data assimilation system

No. 00-15
Mads Hvid Nielsen: Dynamisk beskrivelse og hydrografisk klassifikation af den jyske kyststrøm

No. 00-16
Kristian S. Mogensen, Jess U. Jørgensen, Bjarne Amstrup, Xiaohua Yang and Xiang-Yu Huang: Towards an operational implementation of HIRLAM 3D-VAR at DMI

No. 00-17
Sattler, Kai; Huang, Xiang-Yu: Structure function characteristics for 2 meter temperature and relative humidity in different horizontal resolutions

No. 00-18
Niels Larsen, Ib Steen Mikkelsen, Bjørn M. Knudsen m.fl.: In-situ analysis of aerosols and gases in the polar stratosphere. A contribution to THESEO. Environment and climate research programme. Contract no. ENV4-CT97-0523. Final report

No. 00-19
Amstrup, Bjarne: EUCOS observing system experiments with the DMI HIRLAM optimum interpolation analysis and forecasting system

No. 01-01
V.O. Papitashvili, L.I. Gromova, V.A. Popov and O. Rasmussen: Northern polar cap magnetic activity index PCN: Effective area, universal time, seasonal, and solar cycle variations

No. 01-02
M.E. Gorbunov: Radioholographic methods for processing radio occultation data in multipath regions

No. 01-03
Niels Woetmann Nielsen; Claus Petersen: Calculation of wind gusts in DMI-HIRLAM

No. 01-04
Vladimir Penenko; Alexander Baklanov: Methods of sensitivity theory and inverse modeling for estimation of source parameter and risk/vulnerability areas

No. 01-05
Sergej Zilitinkevich; Alexander Baklanov; Jutta Rost; Ann-Sofi Smedman, Vasiliy Lykosov and Pierluigi Calanca: Diagnostic and prognostic equations for the depth of the stably stratified Ekman boundary layer

No. 01-06
Bjarne Amstrup: Impact of ATOVS AMSU-A radiance data in the DMI-HIRLAM 3D-Var analysis and forecasting system

No. 01-07
Sergej Zilitinkevich; Alexander Baklanov: Calculation of the height of stable boundary layers in operational models

No. 01-08
Vibeke Huess: Sea level variations in the North Sea – from tide gauges, altimetry and modelling

No. 01-09
Alexander Baklanov and Alexander Mahura: Atmospheric transport pathways, vulnerability and possible accidental consequences from nuclear risk sites: methodology for probabilistic atmospheric studies

No. 02-01
Bent Hansen Sass and Claus Petersen: Short range atmospheric forecasts using a nudging procedure to combine analyses of cloud and precipitation with a numerical forecast model

No. 02-02
Erik Buch: Present oceanographic conditions in Greenland waters

No. 02-03
Bjørn M. Knudsen, Signe B. Andersen and Allan Gross: Contribution of the Danish Meteorological Institute to the final report of SAMMOA. CEC contract EVK2-1999-00315: Spring-to.-autumn measurements and modelling of ozone and active species

No. 02-04
Nicolai Kliem: Numerical ocean and sea ice modelling: the area around Cape Farewell (Ph.D. thesis)

No. 02-05
Niels Woetmann Nielsen: The structure and dynamics of the atmospheric boundary layer

No. 02-06
Arne Skov Jensen, Hans-Henrik Benzon and Martin S. Lohmann: A new high resolution method for processing radio occultation data

No. 02-07
Per Høeg and Gottfried Kirchengast: ACE+: Atmosphere and Climate Explorer

No. 02-08
Rashpal Gill: SAR surface cover classification using distribution matching